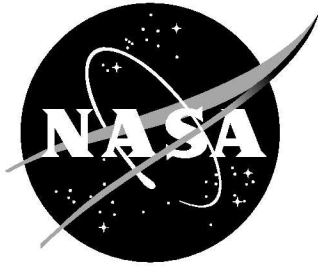


NASA/TP-2009-215951



# Version 2 of the Protuberance Correlations for the Shuttle-Orbiter Boundary Layer Transition Tool

*Rudolph A. King, Michael A. Kegerise and Scott A. Berry  
Langley Research Center, Hampton, Virginia*

---

December 2009

## NASA STI Program . . . in Profile

Since its founding, NASA has been dedicated to the advancement of aeronautics and space science. The NASA scientific and technical information (STI) program plays a key part in helping NASA maintain this important role.

The NASA STI Program operates under the auspices of the Agency Chief Information Officer. It collects, organizes, provides for archiving, and disseminates NASA's STI. The NASA STI Program provides access to the NASA Aeronautics and Space Database and its public interface, the NASA Technical Report Server, thus providing one of the largest collections of aeronautical and space science STI in the world. Results are published in both non-NASA channels and by NASA in the NASA STI Report Series, which includes the following report types:

- **TECHNICAL PUBLICATION.** Reports of completed research or a major significant phase of research that present the results of NASA programs and include extensive data or theoretical analysis. Includes compilations of significant scientific and technical data and information deemed to be of continuing reference value. NASA counterpart of peer-reviewed formal professional papers, but having less stringent limitations on manuscript length and extent of graphic presentations.
- **TECHNICAL MEMORANDUM.** Scientific and technical findings that are preliminary or of specialized interest, e.g., quick release reports, working papers, and bibliographies that contain minimal annotation. Does not contain extensive analysis.
- **CONTRACTOR REPORT.** Scientific and technical findings by NASA-sponsored contractors and grantees.

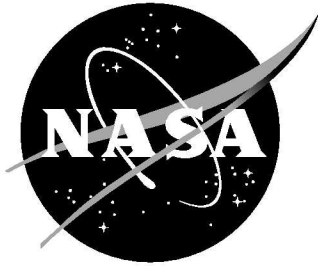
- **CONFERENCE PUBLICATION.** Collected papers from scientific and technical conferences, symposia, seminars, or other meetings sponsored or co-sponsored by NASA.
- **SPECIAL PUBLICATION.** Scientific, technical, or historical information from NASA programs, projects, and missions, often concerned with subjects having substantial public interest.
- **TECHNICAL TRANSLATION.** English-language translations of foreign scientific and technical material pertinent to NASA's mission.

Specialized services also include creating custom thesauri, building customized databases, and organizing and publishing research results.

For more information about the NASA STI Program, see the following:

- Access the NASA STI program home page at <http://www.sti.nasa.gov>
- E-mail your question via the Internet to [help@sti.nasa.gov](mailto:help@sti.nasa.gov)
- Fax your question to the NASA STI Help Desk at 443-757-5803
- Phone the NASA STI Help Desk at 443-757-5802
- Write to:  
NASA STI Help Desk  
NASA Center for AeroSpace Information  
7115 Standard Drive  
Hanover, MD 21076-1320

NASA/TP-2009-215951



# Version 2 of the Protuberance Correlations for the Shuttle-Orbiter Boundary Layer Transition Tool

*Rudolph A. King, Michael A. Kegerise and Scott A. Berry  
Langley Research Center, Hampton, Virginia*

National Aeronautics and  
Space Administration

Langley Research Center  
Hampton, Virginia 23681-2199

---

December 2009

The use of trademarks or names of manufacturers in this report is for accurate reporting and does not constitute an official endorsement, either expressed or implied, of such products or manufacturers by the National Aeronautics and Space Administration.

Available from:

NASA Center for AeroSpace Information  
7115 Standard Drive  
Hanover, MD 21076-1320  
443-757-5802

## Abstract

Orbiter-specific transition data, acquired in four ground-based facilities (LaRC 20-Inch Mach 6 Air Tunnel, LaRC 31-Inch Mach 10 Air Tunnel, LaRC 20-Inch Mach 6 CF<sub>4</sub> Tunnel, and CUBRC LENS-I Shock Tunnel) with three wind tunnel model scales (0.75, 0.90, and 1.8%) and from Orbiter historical flight data, have been analyzed to improve a pre-existing engineering tool for reentry transition prediction on the windward side of the Orbiter. Boundary layer transition (BLT) engineering correlations for transition induced by isolated protuberances are presented using a laminar Navier-Stokes (N-S) database to provide the relevant boundary-layer properties. It is demonstrated that the earlier version of the BLT correlation that had been developed using parameters derived from an engineering boundary-layer code has improved data collapse when developed with the N-S database. Of the new correlations examined, the proposed correlation 5, based on boundary-layer edge and wall properties, was found to provide the best overall correlation metrics when the entire database is employed. The second independent correlation (proposed correlation 7) selected is based on properties within the boundary layer at the protuberance height. The Aeroheating Panel selected a process to derive the recommended coefficients for Version 2 of the BLT Tool. The assumptions and limitations of the recommended protuberance BLT Tool V.2 are presented.

# Contents

|   |           |
|---|-----------|
| <b>List of Tables</b>   | <b>3</b>  |
| <b>List of Figures</b>  | <b>4</b>  |
| <b>1 Introduction</b>   | <b>7</b>  |
| <b>2 Analysis Approach</b>  | <b>8</b>  |
| 2.1 Correlation Analysis . . . . .  | 8         |
| 2.2 Regression Analysis . . . . .   | 9         |
| 2.3 Error Analysis . . . . .  | 10        |
| <b>3 Data Overview</b>  | <b>11</b> |
| 3.1 LaRC 20-Inch Mach 6 Air Tunnel . . . . .  | 12        |
| 3.2 LaRC 31-Inch Mach 10 Air Tunnel . . . . .   | 12        |
| 3.3 LaRC 20-Inch Mach 6 CF <sub>4</sub> Tunnel . . . . .  | 13        |
| 3.4 CUBRC LENS-I Shock Tunnel . . . . .   | 13        |
| 3.5 Historical Flight Data . . . . .  | 14        |
| <b>4 Correlation Results</b>  | <b>14</b> |
| 4.1 LATCH versus N-S Database . . . . .   | 15        |
| 4.2 Proposed Correlations . . . . .   | 16        |
| 4.2.1 PC#1: $Re_{\theta}/M_e = C \times (k/\delta)^n$ . . . . .   | 17        |
| 4.2.2 PC#2 & 3: $Re_{\theta}/M_e = C \times (k/\delta^*)^n$ & $C \times (k/\theta)^n$ . . . . .         | 17        |
| 4.2.3 PC's#4 & 5: $Re_{\theta}/M_e = C/[(k/\delta)(T_e/T_w)^m]$ & $C/[(k/\delta)(H_e/H_w)^m]$ . . . . . | 18        |
| 4.2.4 PC's#6 & 7: $Re_k$ -Type Correlations . . . . .   | 18        |
| 4.3 Correlation Down Select . . . . .   | 19        |
| 4.4 Selection of Correlation Constants . . . . .  | 19        |
| 4.4.1 Option 1 Correlation (PC#5) . . . . .   | 20        |
| 4.4.2 Option 2 Correlation (PC#7) . . . . .   | 21        |
| 4.5 Correlations Revisted . . . . .   | 21        |
| 4.6 Assumptions and Limitations . . . . .   | 22        |
| <b>5 Summary</b>  | <b>23</b> |
| <b>References</b>   | <b>24</b> |

## List of Tables

|    |  |    |
|----|--|----|
| 1  | Relevant correlation parameters for data obtained in the NASA LaRC 20-Inch Mach 6 Tunnel. . . . .  | 26 |
| 1  | Relevant correlation parameters for data obtained in the NASA LaRC 20-Inch Mach 6 Tunnel – (Cont). . . . .   | 27 |
| 2  | Relevant correlation parameters for STS-121mission support data obtained in the NASA LaRC 20-Inch Mach 6 Air Tunnel. . . . .                           | 27 |
| 3  | Relevant correlation parameters for new data obtained in the NASA LaRC 20-Inch Mach 6 Air Tunnel. . . . .  | 28 |
| 4  | Relevant correlation parameters for data obtained in the NASA LaRC 31-Inch Mach 10 Air Tunnel. . . . .   | 29 |
| 5  | Relevant correlation parameters for data obtained in the NASA LaRC 20-Inch CF <sub>4</sub> Tunnel. . . . .   | 30 |
| 6  | Relevant correlation parameters for data obtained at a nominal $M = 10$ in the CUBRC LENS-I Shock Tunnel. . . . .                                      | 31 |
| 7  | Relevant correlation parameters for data obtained at a nominal $M = 16$ in the CUBRC LENS-I Shock Tunnel. . . . .                                      | 31 |
| 8  | Historical flight cases as documented in Refs. [5] and [26]. . . . .   | 32 |
| 9  | Relevant correlation parameters for historical flight cases. . . . .   | 33 |
| 10 | Side-by-side comparison of facility dependent metrics for a correlation in the form of the approved BLT Tool V.1 protuberance correlation. . . . .     | 34 |
| 11 | Down-select table for most promising correlations investigated. . . . .  | 35 |
| 12 | Tabulated correlation coefficients for proposed correlations 5 and 7. . . . .  | 35 |
| 13 | Computed transition times for the ten accepted flight cases using proposed correlations 5 and 7 with the recommended correlation coefficients. . . . . | 36 |
| 14 | Revisited correlations and the respective metrics. . . . .   | 37 |

## List of Figures

|    |   |    |
|----|---|----|
| 1  | Focused inspection image of a protruding gap filler on STS-121. . . . .   | 38 |
| 2  | Generalized correlation approach used in this report. . . . .   | 38 |
| 3  | Complete database (ground-based and flight) projected onto windward surface. . . . .  | 39 |
| 4  | Complete database (ground-based and flight) in the form of $Re_\theta/M_e$ versus $x/L_{ref}$ . . . . .   | 40 |
| 5  | Complete database (ground-based and flight) in the form of $Re_k$ versus $k/\delta$ . . . . .   | 40 |
| 6  | Existing LaRC 20-Inch Mach 6 Air Tunnel data used to develop BLT Tool V.1. . . . .  | 41 |
| 7  | Existing LaRC 20-Inch Mach 6 Air Tunnel data reanalyzed to estimate the incipient transition Reynolds number. . . . .   | 41 |
| 8  | Ensemble of facility dependent data based on N-S database. . . . .  | 42 |
| 9  | Ensemble of facility dependent data based on LATCH database. . . . .  | 42 |
| 10 | Calibrated flight data analyzed using N-S database. . . . .   | 43 |
| 11 | Ensemble of facility dependent data and flight data based on N-S database for correlation $Re_\theta/M_e \times k/\delta = C$ . . . . .                           | 43 |
| 12 | Ensemble of facility dependent data based on N-S database for correlation $Re_\theta/M_e \times k/\delta^* = C$ . . . . .   | 44 |
| 13 | Ensemble of facility dependent data and flight data based on N-S database for correlation $Re_\theta/M_e \times k/\delta^* = C$ . . . . .                         | 44 |
| 14 | Ensemble of facility dependent data and flight data based on N-S database for correlation $Re_\theta/M_e \times k/\theta = C$ . . . . .                           | 45 |
| 15 | Ensemble of facility dependent data and flight data based on N-S database for correlation $Re_\theta/M_e \times (k/\delta)(T_e/T_w)^{0.16} = C$ . . . . .         | 45 |
| 16 | Ensemble of facility dependent data and flight data based on N-S database for correlation $Re_\theta/M_e \times (k/\delta)(H_e/H_w)^{0.30} = C$ . . . . .         | 46 |
| 17 | Ensemble of facility dependent data based on N-S database for correlation $Re_k$ (reference to $\mu_w$ ) = $C$ . . . . .  | 46 |
| 18 | Ensemble of facility dependent data and flight data based on N-S database for correlation of the $Re_k$ -type. . . . .  | 47 |
| 19 | Flight data plotted in correlation space (PC#5) along with correlation curves derived from ensemble of facility dependent and flight data (N-S database). . . . . | 47 |
| 20 | Flight data plotted in correlation space (PC#7) along with correlation curves derived from ensemble of facility dependent and flight data (N-S database). . . . . | 48 |
| 21 | Plot showing flight data and correlation curves with constants recommended by the Aeroheating Panel for PC#5. . . . .   | 48 |
| 22 | Plot showing ground-based data, flight data, and correlation curves for PC#5. . . . .   | 49 |
| 23 | Plot showing flight data and correlation curves with constants recommended by the Aeroheating Panel for PC#7. . . . .   | 49 |
| 24 | Plot showing ground-based data, flight data, and correlation curves for PC#7. . . . .   | 50 |
| 25 | Ensemble of facility dependent data and flight data based on N-S database for correlation $Re_\theta/M_e \times (k/\theta)(H_e/H_w)^{0.44} = C$ . . . . .         | 50 |
| 26 | Plot showing ground-based data, flight data, and derived correlation curves for correlation $Re_\theta/M_e \times (k/\theta)(H_e/H_w)^{0.44} = C$ . . . . .       | 51 |

## Nomenclature

|               |  |
|---------------|--|
| $C$           | Correlation constant (see Eq. 1)   |
| $H$           | Total enthalpy   |
| $k$           | Protuberance height  |
| $L_{ref}$     | Orbiter reference length from nosetip to body-flap hinge line                                |
| $M$           | Mach number  |
| $R$           | Correlation coefficient of regression  |
| $Re$          | unit Reynolds number   |
| $Re_k$        | Reynolds number based on conditions at $k$ , $\rho_k u_k k / \mu_k$                          |
| $Re_\theta$   | Momentum thickness Reynolds number, $\rho_e u_e \theta / \mu_e$                              |
| $S_{\hat{Y}}$ | Standard error of regression   |
| $T$           | Temperature  |
| $u$           | Resultant velocity   |
| $U$           | Uncertainty  |
| $x$           | axial distance from Orbiter nosetip  |
| $X$           | Disturbance parameter (see Eq. 1) or axial distance in Orbiter structural reference system   |
| $y$           | spanwise distance from Orbiter centerline symmetry plane                                     |
| $Y$           | Transition parameter (see Eq. 1) or spanwise distance in Orbiter structural reference system |
| $Z$           | Vertical distance in Orbiter structural reference system                                     |
| $\delta$      | Boundary layer thickness   |
| $\delta^*$    | Displacement thickness   |
| $\theta$      | Momentum thickness   |
| $\mu$         | Viscosity  |
| $\rho$        | Density  |
| $\sigma$      | Standard deviation   |

### *Subscript*

|          |  |
|----------|--|
| 1        | last fully laminar condition           |
| 2        | first condition with laminar departure |
| $e$      | edge conditions                        |
| $flt$    | flight                                 |
| $gb$     | ground based                           |
| $inc$    | incipient conditions                   |
| $k$      | conditions at height $k$               |
| $\infty$ | freestream conditions                  |

### *Superscript*

|                 |                                  |
|-----------------|----------------------------------|
| $n$             | Correlation exponent (see Eq. 1) |
| $m$             | Exponent                         |
| $(\bar{\quad})$ | mean value                       |
| $(\hat{\quad})$ | $= \log(\quad)$                  |

### *Acronyms*

|       |  |
|-------|--|
| BLT   | Boundary layer transition                                |
| CFD   | Computational fluid dynamics                             |
| CUBRC | Calspan-University of Buffalo Research Center            |
| DPLR  | Data-Parallel Line Relaxation                            |
| EI    | Entry interface  |
| LaRC  | Langley Research Center                                  |
| LATCH | Langley Approximate Three-Dimensional Convective Heating |
| LAURA | Langley Aerothermodynamic Upwind Relaxation Algorithm    |
| N-S   | Navier-Stokes  |

PC Proposed correlation  
STS Space Transportation System  
TPS Thermal protection system

# 1 Introduction

The Entry Aeroheating Working Group led by Boeing Houston and NASA Johnson Space Center was created as a result of the Columbia Accident Investigation to develop analysis tools and plans and to execute ground testing in order to monitor the health of the Orbiters thermal protection system (TPS) during reentry. Members of this working group and the associated Aeroheating Panel (see Ref. [1] for details) also provide real-time support to the Damage Assessment Team during each Shuttle mission since STS-107 (STS- Space Transportation System). During Shuttle ascent, the TPS on the Orbiter can experience debris strikes and displacement of TPS components (such as the gap fillers that are placed between the TPS tiles) resulting in cavities and protuberances in the heat shield system. An example of an on-orbit image for a gap filler protruding from the TPS is shown in Figure 1 (image taken during STS-121 mission). This gap filler is somewhat atypical as many rips, tears, and frays are associated with this protuberance (most gap fillers are simply dislodged and do not exhibit rips or tears). Part of the on-orbit process is to determine if cavities and/or protuberances resulting from the ascent stage can cause premature boundary-layer transition resulting in increased thermal loads that can ultimately affect the safety margins during reentry. The Boundary Layer Transition (BLT) Tool, which is one of the suite of tools developed for the Damage Assessment Team, is an engineering tool used in a rapid-turnaround environment to assess if and when these damage sites can cause early transition. The original version of the BLT Tool approved by the Orbiter Project Office in the Space Shuttle Program for this process is Version 1 (see Refs. [1]- [6]).

This report explores potential protuberance correlations to be used for the next-generation Orbiter BLT Tool (Version 2) utilizing ground-based data and calibrated historical flight data (i.e., previous Orbiter flights where protuberance sources were identified as the cause for early boundary-layer transition as inferred from thermocouple measurements) [5]. Proposed correlations due to cavity damages are discussed in a separate report [7]. As a brief recap on the development of the original protuberance correlation, hypersonic boundary-layer transition data were acquired in three ground-based facilities (LaRC 20-Inch Mach 6 Air Tunnel, LaRC 31-Inch Mach 10 Air Tunnel, and LaRC 20-Inch Mach 6 CF<sub>4</sub> Tunnel) on 0.75%-scale wind tunnel models with diamond shaped protuberances. Various correlations were examined using the ground-based measurements and flow parameters derived from an engineering code called LATCH (Langley Approximate Three-Dimensional Convective Heating) [8], which utilized a two-layer approach with inviscid LAURA (Langley Aerothermodynamic Upwind Relaxation Algorithm) [9] solutions. The implementation of LATCH for the BLT Tool V.1 is discussed in Ref. [4]. Most of correlations investigated were not useable due to unsatisfactory data collapse between the three facilities as well as when compared against flight data. Due to these inconsistencies, a simpler correlation utilizing data from one facility, LaRC 20-Inch Mach 6 Air Tunnel, and flight was implemented as the protuberance correlation for the BLT Tool V.1.

There are a few key objectives for the development of a new version of the BLT Tool. Firstly, the LATCH flow properties used in the development of the BLT Tool V.1 are limited to boundary-layer edge properties and wall conditions such that correlations dependent on flow properties within the boundary layer (e.g.,  $Re_k = \rho_k u_k k / \mu_k$  where  $k$  is the height at which these parameters must be defined) are not possible. The first goal was to reexamine the protuberance correlation utilized in BLT Tool V.1 and evaluate alternate correlations using a database derived from full laminar Navier-Stokes solutions. The two viscous CFD solvers used for the present analysis were LAURA [9] and DPLR (Data-Parallel Line Relaxation) [10] codes. The implementation of the viscous CFD database for the next-generation BLT Tool is given in Refs. [11] and [12]. Secondly, the BLT Tool V.1 protuberance correlation was developed using ground-based data obtained in a single facility with a single protuberance type and compared against a few historical flight cases. The correlations pre-

sented herein are developed using a more expansive database to include data obtained in four ground-based facilities and reexamined flight data. This database includes the effects of protuberance shape and orientation, a larger range of trip height normalized by the local boundary-layer thickness ( $k/\delta$ ), and a larger ground-based Mach number range. And lastly, the Orbiter Project Office baselined BLT Tool V.1 protuberance correlation includes only one correlation with no redundancy. So, the final objective was to develop a new protuberance BLT Tool which utilizes two independent correlations, where the primary correlation will be the correlation with the highest level of confidence based on the regression metrics for the entire database (ground-based and flight data).

This report includes a background of the analysis approach, an overview of the protuberance correlation approach (highlighting the protuberance BLT Tool V.1), and a brief review of the entire database. The correlation results are then presented and the findings are summarized. Version 2 of the protuberance BLT Tool approved for future flights by the Orbiter Project Office is presented. From this point forward, reference to the BLT Tool will be synonymous with the protuberance component of the BLT Tool.

## 2 Analysis Approach

In this section, the general correlation and regression analysis will be discussed and will include details of the approved protuberance correlation for the BLT Tool V.1. The general regression approach along with the metrics used for *goodness* of fit will follow. The section closes with a discussion of the error analysis used for the ground-based data.

### 2.1 Correlation Analysis

Transition correlation approaches generally attempt to relate or scale ground-based (wind tunnel and ballistic range) data to flight test conditions. It is important to note that the correlations are not intended to provide a fundamental contribution of the transition physics. Ref. [13] has an extensive review of boundary-layer transition correlation development as it pertains to reentry vehicles. Early correlation results were for the most part based on wetted length transition Reynolds number, but these Reynolds numbers obtained in flight were usually larger than those achieved in ground-based experiments. Also, large data scatter were associated with these results presumably due to factors like local Mach number, wall cooling, surface roughness, wetted length, freestream tunnel disturbance, etc. Later correlations involving Reynolds numbers based on local boundary-layer thicknesses showed marked improvement over those based on wetted length Reynolds numbers. With the advent of high-speed computing, correlations based on reasonably accurate computed local boundary-layer flow properties became practical, particularly for flows that involve entropy layer swallowing dictated by bluntness ratios (e.g., Shuttle Orbiter). The local boundary-layer flow properties are usually computed for laminar flow conditions and these flow and fluid properties are used to develop the correlations. So clearly there is a need for consistent boundary-layer solutions when developing and applying these correlations.

The generalized correlation approach used in this report follows the work summarized in Ref. [14]. Figure 2 shows a schematic of the generalized correlation approach where the abscissa is the logarithm of a disturbance parameter  $X$  and the ordinate the logarithm of a transition parameter  $Y$ . The line in the plot represented by

$$Y = CX^n \tag{1}$$

delineates a *best estimate* boundary for the correlation such that data below the line denote laminar flow and data above denote turbulent flow. For small disturbance parameters  $X$ , the transition parameter  $Y$  should asymptote to a smooth-wall limit, which is facility dependent.

Similarly, for large  $X$  values,  $Y$  asymptotes to a limiting lower value. This limited lower value is referred to as the so called *protuberance limit* (i.e., further increases in roughness height has no additional effect on transition) or a *lower threshold limit* (i.e., the unit Reynolds number is too low to produce and/or maintain the turbulence). Use of a correlation method represents a simplified engineering approach to a complicated physics-based problem. The BLT Tool V.1 was developed using incipient transition data, i.e., data indicating the first evidence of laminar-to-turbulent transition on the windward surface of the Orbiter. The BLT Tool V.1 [2,3] assigns as the disturbance parameter  $X = k/\delta$  where  $k$  is the protuberance height and  $\delta$  the boundary-layer thickness and the transition parameter as  $Y = Re_\theta/M_e$  where  $Re_\theta$  ( $= \rho_e u_e \theta / \mu_e$ ) and  $M_e$  are the momentum thickness Reynolds number and boundary-layer edge Mach number, respectively. The curve coefficient,  $C = 27$ , was selected as a lower bound to the transition Reynolds number data, such that statistically most of the incipient transition data lie above the correlation curve, which introduces some conservatism into the tool. An exponent value of  $n = -1$  was used so that the BLT Tool V.1 is expressed as

$$\frac{Re_\theta}{M_e} \times \frac{k}{\delta} = C. \quad (2)$$

The data used in the development of Eq. 2 are presented later in the report.

## 2.2 Regression Analysis

The power-law form of the generalized correlation can be expressed as

$$\log Y_i = n \log X_i + \log C \quad (3)$$

or

$$\hat{Y}_i = n \hat{X}_i + \hat{C} \quad (4)$$

where  $\hat{Y}_i = \log Y_i$ ,  $\hat{X}_i = \log X_i$  and  $\hat{C} = \log C$ . Applying least-squares regression to Eq. 4 in the  $\hat{X}$ - $\hat{Y}$  space provides expressions for the slope  $n$  and intercept  $\hat{C}$ . The regression equations are

$$n = \frac{N \sum \hat{X}_i \hat{Y}_i - \sum \hat{X}_i \sum \hat{Y}_i}{N \sum \hat{X}_i^2 - (\sum \hat{X}_i)^2} \quad (5)$$

and

$$\hat{C} = \frac{\sum \hat{Y}_i - n \sum \hat{X}_i}{N} \quad (6)$$

where the  $\sum$ 's imply summation from  $i = 1$  to  $N$  with  $N$  being the number of data points. In general, the regression analysis for Eq. 1 has two degrees of freedom to specify the *best fit*, i.e.,  $n$  and  $C$  ( $= 10^{\hat{C}}$ ). If the exponent  $n$  is specified in Eq. 1, then Eq. 5 is replaced by  $n = \text{constant}$  so that there is only one degree of freedom,  $\hat{C}$ . The BLT Tool V.1 is an example where the exponent was specified as a constant, i.e.  $n = -1$ .

The standard error of the regression [15] is given by

$$S_{\hat{Y}} = \left[ \frac{\sum [\hat{Y}_i - (n \hat{X}_i + \hat{C})]^2}{N - 2} \right]^{1/2}. \quad (7)$$

Throughout this document, the upper and lower limits of the 95% confidence limit are assumed to be bounded by the  $2S_{\hat{Y}}$  value about the best fit  $\hat{C}$ . For small sample sizes ( $N < 31$ ), it is more appropriate to assume that the 95% confidence limits for a  $T$ -distribution are bounded by  $tS_{\hat{Y}}$ . Here the numerical value of  $t$  is a function of the sample size  $N$ . For example, ten historical flight cases are discussed in this document. For a sample size of

$N = 10$ , a value of  $t = 2.26$  (1.13 times the assumed value) is the recommended value to provide a 95% confidence limit. Or stated another way, the use of  $2S_{\hat{Y}}$  for the ten flight cases only provides a 92% confidence level. With the above caveat, the upper and lower 95% confidence coefficients assumed in this document (i.e., the  $2S_{\hat{Y}}$  value) in the  $X$ - $Y$  space are

$$C_{+95\%} = 10^{\hat{C} + 2S_{\hat{Y}}} \quad (8)$$

and

$$C_{-95\%} = 10^{\hat{C} - 2S_{\hat{Y}}}, \quad (9)$$

respectively. The correlation constant can be selected to be either  $C_{-95\%}$ ,  $C_{+95\%}$ , or  $C$  with  $C_{-95\%}$  being the most conservative (i.e., with respect to transition prediction capability) and  $C_{+95\%}$  the least conservative constant. As a measure of the *goodness* of the data ( $\hat{X}$  and  $\hat{Y}$ ), the correlation coefficient  $R$  is defined as

$$-1 \leq R = \frac{\sigma_{\hat{X}\hat{Y}}}{\sigma_{\hat{X}}\sigma_{\hat{Y}}} \leq 1 \quad (10)$$

where  $\sigma_{\hat{X}}$  and  $\sigma_{\hat{Y}}$  are the standard deviations of  $\hat{X}$  and  $\hat{Y}$ , respectively, and  $\sigma_{\hat{X}\hat{Y}}$  is the covariance of  $\hat{X}$  and  $\hat{Y}$ . Values of  $|R| \rightarrow 1$  are desirable and implies a strong correlation for the dataset. The other metric used to evaluate the goodness of the regression is

$$\frac{\Delta C}{C} = \frac{C_{+95\%} - C_{-95\%}}{C} \quad (11)$$

where  $\Delta C/C$  is a measure of the scatter in the data about the best fit coefficient  $C$ .

### 2.3 Error Analysis

This section briefly discusses the methodology used to estimate uncertainties incurred in the determination of the disturbance,  $X$ , and transition,  $Y$ , parameters as a result of ground-based measurement uncertainties. The uncertainty analysis is conducted by a Monte Carlo (MC) simulation method [15] and is applied only to the ground-based data. The assumed true value of each input variable is applied to the data reduction equations. All of the associated uncertainties for each of these variables are input. Here, 95% confidence estimates ( $2\sigma$  for Gaussian distributions) are assumed for each uncertainty and a random number generator is used to compute individual error values. The individual error values are added to the corresponding assumed true value of each variable to obtain a *measured* value. The measured values are applied to the data reduction equations to obtain the result variables. The process is repeated  $N_j$  times such that a distribution is obtained for each result variable.

The input uncertainties under consideration here are the Reynolds number uncertainties and uncertainties in the measurement of protuberance height  $k$ . In this report, the assumed true incipient transition unit Reynolds number,  $Re_{\infty,inc}$ , is defined as the average between the last fully laminar value ( $Re_{\infty,1}$ ) and the first non-laminar value ( $Re_{\infty,2}$ ) for all the ground-based data. The values of  $Re_{\infty,1}$  and  $Re_{\infty,2}$  are computed directly from recorded tunnel conditions and have associated uncertainties,  $U_{Re_{\infty,1}}$  and  $U_{Re_{\infty,2}}$ . These uncertainties are represented by a Gaussian distribution such that  $U_{Re_{\infty}} = 2\sigma_{Re_{\infty}}$ . The incipient transition Reynolds number for realization “ $j$ ” is in the range  $Re_{\infty,1}^{(j)} \leq Re_{\infty,inc}^{(j)} \leq Re_{\infty,2}^{(j)}$  provided that the uncertainties  $U_{Re_{\infty,1}}$  and  $U_{Re_{\infty,2}}$  are much less than the percent difference between  $Re_{\infty,1}$  and  $Re_{\infty,2}$  (typically larger than 20%). A uniform distribution is assumed for the *measured*  $Re_{\infty,inc}^{(j)}$  since this value is equally likely to be any value in the interval between  $Re_{\infty,1}^{(j)}$  and  $Re_{\infty,2}^{(j)}$ . The uncertainties for the protuberance height  $k$  are represented

by a Gaussian distribution where  $U_k = 2\sigma_k$ . The measured value,  $k^{(j)}$ , is the assumed true  $k$  value plus the individual uncertainty for each “ $j$ ” realization.

The nominal Reynolds number percent uncertainty (based on the range of  $Re_{\infty,inc}$  tested) used for NASA Langley Research Center’s 20-Inch Mach 6 Air Tunnel is estimated at 3% based on data reported in Ref. [16]. Similarly, nominal Reynolds number uncertainty for the NASA Langley Research Center’s 31-Inch Mach 10 Air Tunnel is estimated at 1.2% based on unpublished data.<sup>1</sup> No information was available for the other NASA facility, the 20-Inch Mach 6 CF<sub>4</sub> Tunnel, so the nominal value was assumed to be the same as that for the 20-Inch Mach 6 Air Tunnel (i.e., 3%). For the CUBRC LENS-I Shock Tunnel, the nominal Reynolds number percent uncertainties estimated are 4% and 5% for Mach 10 and Mach 16, respectively [17]. These values are considerably less than the percent difference values between  $Re_{\infty,1}$  and  $Re_{\infty,2}$ . The uncertainty used for the protuberance height  $k$  in all measurements is estimated to be  $U_k = 0.0005$  in. based on repeated measurements. All error analysis presented in this document were conducted using  $N_j = 500,000$  realizations. Take as an example the BLT Tool V.1, the flow properties in both  $X (= k/\delta)$  and  $Y (= Re_{\theta}/M_e)$  have been approximately scaled relative to Reynolds number. The flow properties at the assumed true value,  $Re_{\infty,inc}$ , are known, thus a scaling relationship is required to obtain the results in flow properties based on uncertainties in  $Re_{\infty}$ . The values of  $Re_{\theta}/M_e$  and  $\delta$  are thus scaled using

$$\frac{Re_{\theta}}{M_e} = \frac{Re_{\theta,inc}}{M_e} \times \sqrt{\frac{Re_{\infty}}{Re_{\infty,inc}}} \quad (12)$$

and

$$\delta = \delta_{inc} \times \sqrt{\frac{Re_{\infty,inc}}{Re_{\infty}}}, \quad (13)$$

respectively. Distributions of  $(Re_{\theta}/M_e)^{(j)}$  and  $k^{(j)}/\delta^{(j)}$  are obtained using these techniques and the corresponding uncertainties,  $U_{Re_{\theta}/M_e}$  and  $U_{k/\delta}$ , are computed based on  $2\sigma$  values.

### 3 Data Overview

The data used to develop the correlations in this report were obtained in four ground-based facilities and on several historical Shuttle missions. The bulk of the data to be presented were based on measurements obtained in NASA Langley Research Center (LaRC) Aerothermodynamic Laboratory (LAL) which consist of three hypersonic wind tunnels [18]. The three tunnels are the 20-Inch Mach 6 Air Tunnel, the 20-Inch Mach 6 CF<sub>4</sub> Tunnel, and the 31-Inch Mach 10 Air Tunnel. The high Mach number ground-based data were obtained in the Calspan-University of Buffalo Research Center (CUBRC) LENS-I Shock Tunnel [17, 19]. The ground-based transition data were derived from heat transfer measurements. A departure in the normalized mean heat transfer rate from the laminar baseline was used as the primary transition criterion. The ground-based tests were conducted over a range of unit Reynolds numbers as the heat transfer measurements were acquired to evaluate the state of the boundary-layer flow. As discussed already in the Section 2.3, an estimate of the incipient transition unit Reynolds number,  $Re_{\infty,inc} (= \rho_{\infty}u_{\infty}/\mu_{\infty})$ , is defined as the average Reynolds number between the last fully laminar condition ( $Re_{\infty,1}$ ) and the first condition with evidence of laminar departure ( $Re_{\infty,2}$ ). This basis for defining the incipient conditions will be used throughout this document. The results to be presented as part of the BLT Tool V.2 development were derived from the N-S database extraction tool [11] using the experimental test conditions as inputs. The N-S solutions are fully laminar solutions on a smooth Orbiter geometry (i.e., without the protuberances). All the ground-based data

<sup>1</sup>Rhode, M. N., Private communication, January 2007.

reported in this document were acquired at a nominal angle of attack of 30° or 40° and a nominal yaw angle of 0°.

### 3.1 LaRC 20-Inch Mach 6 Air Tunnel

The existing  $M = 6$  data obtained prior to the development of the BLT Tool V.1 are presented in Table 1. The measurements were acquired on 0.75%-scale Orbiter models. Most of the data were acquired at a nominal angle of attack of 40° and a few cases at 30°. A phosphor thermography system was used to infer global heat transfer rates on the windward model surface for hypersonic boundary-layer transition detection. Details of the experimental setup and test conditions are available in Ref. [20]. The flow parameters presented in the table are those required for the correlations examined during this study. For the coordinate system given in the table, axial distance from the nosetip is represented by  $x$  and spanwise distance from the centerline (CL) symmetry plane is  $y$ . The flow properties are probed at  $(x/L_{ref}, y/L_{ref})$  which corresponds to the location of the protuberances (diamond-shaped trips for this database) with heights  $k$ . The data in Table 1 correspond to those at the estimated incipient transition Reynolds number (based on the average between the last fully laminar value and first value with laminar departure). The test conditions for the data presented on the first page of this table (first 30 data points) were the only ground-based conditions used in the development of the BLT Tool V.1. The range of the current disturbance parameter for this Mach 6 data is  $0.2 \leq k/\delta \leq 1.6$  based on the N-S database. All  $k/\delta$  values reported in this section were derived from the N-S database.

The data presented in Table 2 were obtained in support of the STS-121 mission on a 0.75%-scale Orbiter model at a nominal angle of attack of 40°. All transition measurements were acquired with raised diamond-shaped (“pizza-box”) trips at  $x/L$  locations more aft than the previous data. Details of the experimental setup and test conditions are provided in Ref. [21]. Later in the document, the combined test conditions characterized in Tables 1 and 2 are referred to as “existing Mach 6 data.” The range of  $k/\delta$  for the STS-121 mission support data is  $0.2 \leq k/\delta \leq 0.5$ .

Table 3 presents recently acquired Mach 6 data obtained as part of a technical expert investigation study. The funding was allocated to the BLT Team as a discretionary resource to support potential studies that the team deemed important with concurrence from the Aeroheating Panel. The BLT Team decided to use the resources to conduct a protuberance study, and this data will be referred to as the new Mach 6 data. The measurements were acquired on 0.9%-scale Orbiter models at a nominal angle of attack of 40°. The larger model scale (20% larger than the 0.75%-scale model) facilitated improved manufacturing capabilities of the protuberance geometry and size. The data expanded the existing Mach 6 database by acquiring data for other representative protuberance shapes (e.g., gap fillers and shapes resulting from tile repair concepts), for protuberances at aft locations on the Orbiter and for protuberances at outboard locations inboard of the shock interaction region. Details of the experimental setup, test conditions, and results are provided in Ref. [22]. The range of  $k/\delta$  for the new data is  $0.2 \leq k/\delta \leq 0.6$ .

In summary, all the Mach 6 data were acquired for protuberance heights in the range of  $0.2 \leq k/\delta \leq 1.6$ . The corresponding boundary-layer edge to wall temperature ratios for these conditions at the location of the trips are in the range  $0.7 \leq T_e/T_w \leq 1.4$ .

### 3.2 LaRC 31-Inch Mach 10 Air Tunnel

The existing  $M = 10$  data obtained prior to the development of the BLT Tool V.1 are presented in Table 4. The transition measurements were acquired on 0.75%-scale Orbiter models using a phosphor thermography system. Most of the measurements were acquired at a nominal angle of attack of 40° and a few cases at 30°. In all cases, transition was forced

with raised diamond-shaped protuberances. Details of the experimental setup and test conditions are available in Ref. [20]. These  $M = 10$  data were not used in the development of the BLT Tool V.1 derived with the LATCH database due to unsatisfactory collapse in the correlation space with the  $M = 6$  data and historical flight data. However, the BLT Tool V.2 includes these data and it will be shown that use of a N-S database for the correlation parameters leads to an acceptable data collapse. The range of  $k/\delta$  for the Mach 10 data is  $0.2 \leq k/\delta \leq 2.1$ . The temperature ratios are in the range  $1.6 \leq T_e/T_w \leq 2.4$ , larger than the ratios at Mach 6.

### 3.3 LaRC 20-Inch Mach 6 CF<sub>4</sub> Tunnel

The LaRC 20-Inch Mach 6 CF<sub>4</sub> Tunnel uses tetrafluoromethane (CF<sub>4</sub>) as the test gas. CF<sub>4</sub> has a larger normal shock density ratio and smaller ratio of specific heats ( $\gamma$ ) than air. This simulates an important aspect of dissociative high-temperature effects associated with the reentry of blunt vehicles, i.e., the increase in normal shock density ratio or the decrease in the ratio of specific heats that occurs within the shock layer of the vehicle [23]. Existing Mach 6 CF<sub>4</sub> data are presented in Table 5 for data acquired on 0.75%-scale Orbiter models with raised diamond-shaped protuberances. Most of the data were acquired at a nominal angle of attack of 40° and a few cases at 30°. Heat transfer data were inferred using a phosphor thermography system. Details of the experimental setup and test conditions are available in Ref. [20]. These data were not used as part of the development of the BLT Tool V.1 derived with the LATCH database due to unsatisfactory collapse in the correlation space of the database with the  $M = 6$  data and historical flight data. As for the case with data acquired in the LaRC 31-Inch Mach 10 Air Tunnel, the BLT Tool V.2 will include the CF<sub>4</sub> database when the N-S database is used for the deriving the correlation parameters. The range of  $k/\delta$  for the CF<sub>4</sub> data is  $0.2 \leq k/\delta \leq 2.7$ . The corresponding temperature ratios are  $1.3 \leq T_e/T_w \leq 1.8$  and tend to bridge the range between the LaRC Mach 6 and Mach 10 Air Tunnels.

### 3.4 CUBRC LENS-I Shock Tunnel

Recently acquired transition data were obtained at Mach 10 and 16 in the LENS-I Shock Tunnel on a 1.8%-scale Orbiter model. Data were acquired for protuberance shapes in the form of raised diamond-shaped trips and fence trips. All of the data were acquired at a nominal angle of attack of 40°. Heat transfer measurements, inferred by thin-film gauges, and temperature sensitive paint measurements were used to assess the state of the flow. The data collected in the CUBRC facility extended both the ground-based Mach number and  $k/\delta$  ranges. Details of the experimental setup, test conditions, and results are available in Ref. [24] (see also Ref. [25] for experimental setup). The Mach 10 data are presented in Table 6 where the range of  $k/\delta$  is  $0.3 \leq k/\delta \leq 0.4$  and  $T_e/T_w$  is  $2.7 \leq T_e/T_w \leq 2.8$  (somewhat larger temperature ratios than the LaRC Mach 10 Air Tunnel). Two Mach 16 test cases (configurations 4 and 5 as noted in Ref. [24]) were tested at large  $k/\delta$  values in order to acquire transition onset data at low unit  $Re_\infty$ 's. Transition onset due to both starboard and port attachment-line trips was not realized for configuration 4 but, based on supplementary measurements (i.e., unsteady heat transfer data), transition appeared to be imminent (see Ref. [24] for discussion). Table 7 presents the correlation parameters for the Mach 16 data. The last two lines of Table 7 provide the properties at the highest unit  $Re_\infty$  tested for the laminar attachment-line flow for configuration 4. These laminar results are documented in the table for the purpose of qualitative interpretation (to be discussed later). The range of  $k/\delta$  for the Mach 16 data is  $0.2 \leq k/\delta \leq 3.5$ . The temperature ratios are significantly larger than those for the other ground-based facilities, namely  $4.9 \leq T_e/T_w \leq 5.4$

### 3.5 Historical Flight Data

Actual flight data are essential to calibrate and anchor the BLT Tool as the ground-based data cannot accurately simulate the reentry atmospheric conditions experienced by the Orbiter. As a result, historical flight data were reexamined to better determine the root causes of the occasional early transition times realized on some of the past Shuttle missions. Details of the analysis are given in Ref. [5] and further refined in Ref. [26]. Ten flight cases were identified as having early transition times due to protruding gap fillers: STS-28 (2 cases), STS-41, STS-55 (2 cases), STS-73, STS-81, STS-94, STS-99 and STS-103. These flight cases are tabulated in Table 8 along with their respective measured transition times from entry interface, EI (EI is arbitrarily defined as the altitude at which the Orbiter enters the discernible atmosphere at 400,000 feet). In the Orbiter structural reference system given in this table, axial distance is represented by  $X$  ( $X = 236$  in. represents the nosetip), spanwise distance from the centerline symmetry plane is  $Y$ , and distance in the vertical direction is characterized by  $Z$  ( $Z = 338.5$  in. represents the nosetip). The estimated uncertainties in the post-flight measurements of the gap filler protrusion heights,  $k$ , are also indicated in the table and provide a measure of uncertainty for the flight data. The reported uncertainties in  $k$  were obtained from different sources and methodologies (refer to Ref. [26] for details). Note that three interpretations are available for STS-73. The gap filler for STS-73 was bent over during post-flight measurements with a bent over height of  $k = 0.6$  in. and an unbent height of  $k = 1.4$  in. Also, two likely transition times were extracted from the thermocouple data detected on the windward surface of the Orbiter (refer to Refs. [5] and [26] for more details). The interpretation accepted by the Aeroheating Panel is the first STS-73 line shown in the table which assumes a  $k$  consistent with the bent height and the earlier of the two transition times from EI (880 seconds). The two alternate interpretations are indicated in the table with asterisks for completeness. The relevant correlation parameters are presented in Table 9 where  $x$  is the axial distance from the nosetip of the Orbiter. The range of  $k/\delta$  for the historical flight cases is  $0.1 \leq k/\delta \leq 0.3$ , i.e., all submerged protuberances. The corresponding range in freestream Mach number is  $7 \leq M \leq 19$ . The corresponding temperature ratios are  $2.6 \leq T_e/T_w \leq 4.3$ , which are bracketed by the ground-based values.

## 4 Correlation Results

In this section, the BLT Tool V.1 protuberance correlation is compared using the LATCH and Navier-Stokes databases. Proposed correlations are then presented followed by a down-select process. The agreed upon correlation constants for the down-selected correlations are presented. Assumptions and limitations of the down-select correlations are discussed.

Before proceeding, three graphical illustrations of all the data to be used in the development of the next-generation BLT Tool are shown in Figures 3 through 5. The first plot, Figure 3, overlays the database onto the Orbiter's windward surface. The existing databases (LaRC's M6, M10 & CF<sub>4</sub> data) use only positive  $y/L_{ref}$  values, but data were acquired with protuberances on both the starboard and port sides of the Orbiter. For the other databases, positive  $y/L_{ref}$  values denote the starboard side and negative  $y/L_{ref}$  values denote the port side. The historical flight data (plotted as  $y/L_{ref} > 0$ ) are all captured within the spatial extent of the ground-based data. The plot of N-S based  $Re_\theta/M_e$  versus the normalized streamwise coordinate  $x/L_{ref}$  in Figure 4 demonstrates the range of the experimental data. Some values of  $Re_\theta/M_e$  for flight are larger than those for the ground-based data. Similarly, Figure 5 shows a plot of N-S based  $Re_k (= \rho_k u_k k / \mu_k)$  versus  $k/\delta$  where the subscript ' $k$ ' denotes that the properties are evaluated at the trip height  $k$ . It should be noted that not all the data are for submerged protuberances ( $k/\delta < 1$ ), since the relevance of  $Re_k$  for protuberances larger than the local boundary thickness is unclear. The values of  $Re_k$  for

flight are larger than the corresponding ground-based data at similar  $k/\delta$  values; however, the overall  $Re_k$  values for flight are within the range of those obtained in the ground-based facilities. Note that the use of correlations in the format of  $Re_\theta/M_e$  and/or  $Re_k$  equal a constant, demonstrate uncertainties more than a factor of ten for the Orbiter’s windward surface. Due to this large uncertainty, the correlations used in the BLT Tool V.1, and those implemented for the BLT Tool V.2 have additional correlating parameters to mitigate large uncertainties.

#### 4.1 LATCH versus N-S Database

The data analysis done in this report is slightly different from the analysis done in the development of the BLT Tool V.1 [2, 3]. As noted earlier, the incipient transition unit Reynolds number,  $Re_{\infty,inc}$ , in this report is defined as the average between the last fully laminar value ( $Re_{\infty,1}$ ) and the first non-laminar value ( $Re_{\infty,2}$ ) for all the ground-based data. With this consistent framework, the percent error between the actual and estimated  $Re_{\infty,inc}$  is bounded by one-half the percent difference between  $Re_{\infty,1}$  and  $Re_{\infty,2}$ . For the development of the BLT Tool V.1, a different approach was used, in which  $Re_{\infty,inc}$  was usually taken as the last laminar value. With that approach, the percent error in  $Re_{\infty,inc}$  can be as large as the percent difference between  $Re_{\infty,1}$  and  $Re_{\infty,2}$ , and the estimated  $Re_{\infty,inc}$  values are consistently biased to low values. The percent difference between  $Re_{\infty,1}$  and  $Re_{\infty,2}$  in some cases can be as large as 50%. Plots showing both approaches are shown in Figures 6 and 7 where  $C$  (“Best Fit”) refers to the best estimate of the regression fit. The data plotted are based on the LATCH solutions and are the only ground-based data used to develop the BLT Tool V.1. Using the previous framework for estimating  $Re_{\infty,inc}$  (see Figure 6), the best fit and  $-2\sigma$  fit are  $C = 38.6$  and  $C_{-95\%} = 28.4$ , respectively. The accepted coefficient for Version 1 is  $C = 27$  which was selected as the conservative bound akin to the  $C_{-95\%}$  coefficient value of 28.4 in this analysis. A percent difference of 5% between these two coefficients is realized and is mainly attributed to the analysis used, i.e., the Version 1 analysis used a trial and error approach to conservatively bound the results versus the more rigorous regression approach applied here. Using the current framework (see Figure 7), the corresponding values are  $C = 40.4$  and  $C_{-95\%} = 27.8$ . This translates to a 4.6% and a 2.1% difference in  $C$  and  $C_{-95\%}$  between both frameworks. The uncertainties represented by the cross-hairs in the Figure 7 are from contributions due to the uncertainties in  $Re_{\infty,inc}$  as discussed in Section 2.3 (computed using MC method). The error bars here are used to demonstrate that the consistent analysis approach introduces uncertainties that are bounded for the most part by the 95% confidence levels of the data. The uncertainty in  $k$  was set to zero ( $U_k = 0$ ) since only the contributions due to the uncertainties in Reynolds numbers were intended. From this point forward, the consistent framework to estimate  $Re_{\infty,inc}$  is used exclusively.

Correlation plots for the ensemble of the ground-based data are shown in Figures 8 and 9 for the N-S and LATCH databases, respectively. The plots include error bars to denote resulting uncertainties in  $Re_\theta/M_e$  and  $k/\delta$  (refer to Section 2.3 for discussion). These uncertainties account for uncertainty contributions due to  $Re_{\infty,inc}$  selection and protuberance height,  $k$ , measurements. An estimated uncertainty in  $k$  based on measurements is taken as  $U_k = \pm 0.0005$  in. for all ground-based data. Note that the scatter is larger for the new Mach 6 data than for the existing Mach 6 data using both the N-S and LATCH databases. Protuberance shape effects and orientation effects were investigated in the new study thereby increasing the variability in the data. Protuberance orientation effects on  $Re_{\infty,inc}$  could be significant but no first-order shape effects were realized (refer to Ref. [22] for details). Significant variability also exist for the LENS-I Mach 16 data. The circled data points on the right of the plot (4 data points but appear as 3 data points) were obtained for large  $k/\delta$  ( $> 1.3$ ) values. The inference was made in Ref [24] that these low  $Re_\infty$  conditions tend to suggest a

lower threshold at Mach 16 necessary to sustain turbulent flow. The regression analysis for the ensemble data do not include the four LENS-I Mach 16 data points at  $k/\delta > 1.3$ . These data points will introduce some bias into the results as  $Re_\theta/M_e$  asymptotes to a threshold limit for large  $k/\delta$  values. Both measures of *goodness*,  $R$  and  $\Delta C/C$ , show improvement from the LATCH framework to the N-S framework. Table 10 shows a comparison of the facility dependent metrics between the LATCH and N-S databases. Overall improvement in the metrics (decrease in  $\Delta C/C$  and increase in  $|R|$ ) is observed for the N-S database except for the LENS-I Mach 16 data. A new ensemble metric,  $\sigma_C/\bar{C}$ , is introduced in the table where  $\sigma_C$  is the sample standard deviation and  $\bar{C}$  the mean of the facility constants. Note that this new measure is only applied when each facility regression uses the same numeric value for  $n$ . The calculation of  $\sigma_C/\bar{C}$  does not include the LENS-I Mach 16 data since the regression fit is flawed (see comment above). This metric is a measure of the facility-to-facility regression variability. Again, the N-S database show better results than the LATCH database, i.e., reduced variability.

A plot of the historical flight data in the correlation space is presented for completeness in Figure 10. Each datum has the associated STS mission identified in the figure. The ten flight cases accepted by the Aeroheating Panel are shown along with the two alternate interpretations of STS-73 (refer to Section 3.5 for details). The metrics,  $R$  and  $\Delta C/C$ , are computed based on the ten accepted flight cases. Recall from the discussion in Section 2.2 for small sample sizes that it is more appropriate to assume a  $T$ -distribution for the 95% confidence limits, i.e.,  $\pm t S_{\hat{y}}$  uncertainty band. If  $t = 2.26$  is assumed for  $N = 10$ , then  $(C_{-95\%}, C_{+95\%}) = (31.1, 55.6)$  instead of  $(C_{-95\%}, C_{+95\%}) = (32.2, 53.8)$  as reported in the figure. It is evident that the percent differences in the confidence limits are small (less than 3.5%), and thus supports the assumption of using a consistent value of  $t = 2$  in this report as appropriate. The horizontal error bars shown in the plot represent the uncertainties in protrusion heights,  $k$  (see Table 8). Based on the available documentation, it is not clear if the uncertainties in  $k$  are representative of a 95% uncertainty band, a value typically used in engineering applications. Throughout this baselining process, 95% confidence limits have been used for the uncertainties. Recall that for a Gaussian distribution, the 95% confidence limits are consistent with  $\pm 2\sigma$  uncertainties about the mean. Similarly,  $\pm\sigma$  uncertainties are representative of 68% confidence limits. However, based on the relative magnitudes of some of these uncertainty values given in Table 8, the values do not appear to have a consistent uncertainty basis. All but two of the uncertainties quoted for the accepted flight cases are greater than  $\pm 18\%$ ; hence, the quoted uncertainty bands are most likely representative of 95% confidence limits ( $\pm 2\sigma$ ) than, for example, 68% confidence limits ( $\pm\sigma$ ). The uncertainties in transition times reported in Refs. [5] and [26] are less than a few seconds. These time uncertainties represent small percent errors in  $Re_\theta/M_e$  and  $\delta$  and consequently were not included in the flight uncertainty analysis. The error bars shown in Figure 10 assumes the  $k$  uncertainties in Table 8 represent 95% confidence levels.

## 4.2 Proposed Correlations

All proposed correlations, PC, are developed using the Navier-Stoke database. For all the proposed correlations, the regression analysis for the ensemble data, both with and without flight data, does not include the LENS-I Mach 16 data for  $k/\delta > 1.3$  (see discussion in Section 4.1). As a reminder, these excluded transition onset data points are circled red in the correlation plots to follow. Data points for the laminar LENS-I Mach 16 data (refer to Section 3.4) are enclosed using a green circle with a tail when plotted. The laminar data (two data points but appear as one) are obviously not used in the regression analysis but are presented to reinforce the observed departure of the large  $k/\delta$ , Mach 16 data from those at lower Mach numbers.

Various correlating parameters were examined that took advantage of the fluid and flow variables available or derivable from the existing N-S database. Correlations were assessed for the ensemble of ground-based data as well as for the entire database (ground-based + flight data). A representation of the correlations investigated are discussed below. In addition, protuberance correlations with independent correlating parameters were examined to achieve the goal of obtaining redundant independent correlations. The primary protuberance correlation will be the correlation with the highest level of confidence based on the regression metrics for the entire database. In the following subsections, the reader will be pointed to correlation plots that include some of the regression metrics but not the ensemble metric,  $\sigma_C/\bar{C}$ . These are summarized in Table 11.

#### 4.2.1 PC#1: $Re_\theta/M_e = C \times (k/\delta)^n$

The form of the BLT Tool V.1 correlation with all the ground-based and historical flight data is presented in Figure 11. This correlation will serve as a baseline for future comparison. For the plot shown, the exponent was kept constant,  $n = -1$ . A value of  $n = -1.04$  for the exponent was obtained when it was allowed to vary in the regression analysis. The flight data are bounded by the best fit curve,  $C = 32.6$ , and the least conservative curve,  $C_{+95\%} = 58.8$ . Note that the transition onset Mach 16 data for  $k/\delta > 1.3$  (symbols enclosed with red circles) depart from the observed trends of the lower Mach number data. Similarly, the laminar Mach 16 data for  $k/\delta \approx 1.8$  (symbols enclosed with a green circle) also support the observed trends and are in the same family as the transition onset Mach 16 data for large  $k/\delta$ . The ensemble metric for this database (ground-based and flight data) is  $\sigma_C/\bar{C} = 21.2\%$ .

#### 4.2.2 PC#2 & 3: $Re_\theta/M_e = C \times (k/\delta^*)^n$ & $C \times (k/\theta)^n$

For hypersonic flows, the boundary-layer thickness,  $\delta$ , can be overly sensitive to the methodology used to define the boundary-layer edge [27]. Also, it was thought that the displacement thickness,  $\delta^*$ , or momentum thickness,  $\theta$ , may provide some level of improved facility-to-facility collapse as they account, somewhat indirectly, for temperature differences between the facilities. As a first attempt, the disturbance parameter was changed to  $X = k/\delta^*$  to mitigate the sensitivity observed with  $\delta$ . As before, the exponent was assumed constant,  $n = -1$  (a value of  $n = -0.96$  was obtained for the entire database when  $n$  was allowed to vary in the regression analysis). A plot of the proposed correlation, for ground-based data only, is presented in Figure 12. The ensemble metric for this correlation is  $\sigma_C/\bar{C} = 7.3\%$ . This correlation clearly demonstrates better collapse of the ground-based data when compared with the baseline correlation in Figure 8 where  $\sigma_C/\bar{C} = 19.9\%$ . When the flight data is added to the database as shown in Figure 13 (the ensemble metric increases to  $\sigma_C/\bar{C} = 34.9\%$ ), the proposed correlation becomes less attractive when compared to the baseline in Figure 11. All the metrics,  $\Delta C/C$ ,  $|R|$ , and  $\sigma_C/\bar{C}$ , indicate a less robust correlation than that of the baseline when both ground-based and flight data are utilized. Whether this ground-based versus flight data discrepancy should be attributed to differences in test versus flight environment, or some other factor, is unclear.

As a second attempt, the disturbance parameter was changed to  $X = k/\theta$  to mitigate the sensitivity observed with  $\delta$ . Again, the exponent was assumed constant,  $n = -1$  ( $n = -0.92$  was obtained for the entire database in the regression analysis). A plot of the proposed correlation for the ground-based and flight data is presented in Figure 14. The ensemble metric for this correlation is  $\sigma_C/\bar{C} = 23.3\%$ , slightly larger than the baseline value of  $\sigma_C/\bar{C} = 21.2\%$  (see Figure 11). All the metrics,  $\Delta C/C$ ,  $|R|$ , and  $\sigma_C/\bar{C}$ , indicate a less robust correlation than that of the baseline when both ground-based and flight data are utilized.

#### 4.2.3 PC's#4 & 5: $Re_\theta/M_e = C/[(k/\delta)(T_e/T_w)^m]$ & $C/[(k/\delta)(H_e/H_w)^m]$

The next correlation approach investigated the implementation of either a temperature ratio,  $T_e/T_w$ , or total enthalpy ratio,  $H_e/H_w$ , to mitigate the facility variability. At the time the BLT Tool V.2 was being developed, the decision was made to implement this approach with the most promising of the proposed correlations. As a result, this implementation was conducted for PC#1. To obtain values of the exponent  $m$  that provided *best* values of the metrics, the regression was conducted recursively for values of the exponent in the range  $-1 \leq m \leq 1$ . Note that a value of  $n = -1$  was used for the regression exponent. The values of  $m$  using both the ground-based and flight data for  $T_e/T_w$  and  $H_e/H_w$ , which yielded the lowest values of  $\Delta C/C$ , were found to be  $m = 0.16$  and  $m = 0.30$ , respectively. Figure 15, which includes both ground-based and flight data, shows the correlation plot for the disturbance parameter  $X = [(k/\delta)(T_e/T_w)^m]$  where  $\sigma_C/\bar{C} = 23.6\%$ . A similar plot using the total enthalpy ratio is presented in Figure 16. The ensemble metric using the total enthalpy ratio is  $\sigma_C/\bar{C} = 19.9\%$ . All the metrics ( $\Delta C/C$ ,  $|R|$ , and  $\sigma_C/\bar{C}$ ) for the correlation with disturbance parameter,  $X = [(k/\delta)(H_e/H_w)^m]$ , are better than both the baseline correlation (PC#1) and the correlation with  $X = [(k/\delta)(T_e/T_w)^m]$  when both the ground-based and flight data are utilized.

#### 4.2.4 PC's#6 & 7: $Re_k$ -Type Correlations

In the first correlation considered in this section, the disturbance and transition parameters were selected as  $X = (\rho_k u_k k)/(\rho_e u_e \theta)$  and  $Y = \rho_e u_e \theta/\mu_w$ , respectively [14]. The subscripts 'k' and 'w' denote properties evaluated at height  $k$  in the undisturbed laminar boundary layer and at the wall, respectively. The correlation was evaluated with an exponent  $n = -1$  (i.e.,  $\rho_k u_k k/\mu_w = C$ ) using all the ground-based data and is shown in Figure 17. It becomes obvious looking at the plot and metrics that an exponent of  $n = -1$  is not appropriate. The metrics for this correlation are undesirable (relatively large  $\Delta C/C$  and small  $|R|$ ) and do not improve significantly if  $n$  becomes a free parameter in the regression analysis. With the addition of the flight data, the metrics for this correlation become worse. As a result, this correlation approach was not pursued further. Ref [14] shows a similar plot (Figure 2 in the reference) with data reported in Ref [28] that were obtained only on the centerline of a Shuttle-Orbiter model. The plot reported there shows a good correlation, unlike the data presented here. Note that the best fit constants for both plots are in excellent agreement ( $C = 343$  for the current data and  $C = 344$  for the data reported in Ref [14]), which serves as a sanity check for the current analysis. It should be noted that the current data includes results obtained away from the centerline in the influence of crossflow. Additionally, data with  $k/\delta > 1$  are also part of the current dataset and the interpretation of  $Re_k$ -type correlations for protuberances extending beyond the boundary layer is unclear.

The next correlation considered defines as the disturbance and transition parameters  $X = (\rho_k u_k k)/(\rho_e u_e \theta)$  and  $Y = \rho_e u_e \theta/\mu_k$ , respectively. Note that the only difference between this correlation and the previous correlation is the location at which the viscosity is evaluated (at height  $k$  versus at the wall). Substituting into Eq. 1 gives the following expression,

$$Re_k^{-n} \times \left[ Re_\theta \cdot \left( \frac{\mu_e}{\mu_k} \right) \right]^{1+n} = C. \quad (14)$$

For the special case of  $n = -1$ , Eq. 14 degenerates to  $Re_k = C$ , the scenario discussed in Ref [14]. Figure 18, which includes ground-based and flight data, presents the correlation plot where the exponent was selected as  $n = -0.6$  (best fit exponent,  $n = -0.573$ , rounded to nearest tenth). The ensemble metric is  $\sigma_C/\bar{C} = 35.0\%$ , larger than the baseline value of  $\sigma_C/\bar{C} = 21.2\%$  (refer to in Figure 11). The flight data are biased toward the  $C_{+95\%}$

line. Note that the large  $k/\delta$ , LENS-I Mach 16 data fall within the 95% confidence limits unlike the previous correlations. It is not clear why the large  $k/\delta$  data are in family for this correlation.

### 4.3 Correlation Down Select

The correlations are summarized in the Table 11. Based on the correlation metrics, proposed correlation 5 provides the best collapse of the total ensemble data (ground-based + flight). Proposed correlations 1 - 5 are not sufficiently independent correlations since they share the same disturbance parameter  $Re_\theta/M_e$ . Consequently, PC#7 is the next best independent correlation based on the correlation metrics in the table. The recommended engineering correlations for the next-generation BLT Tool are therefore proposed correlations 5 and 7, where PC#5 uses an  $Re_\theta/M_e$  versus  $(k/\delta) \cdot (H_e/H_w)^{0.30}$  correlation, and PC#7 an  $\rho_e u_e \theta / \mu_k$  versus  $(\rho_k u_k k) / (\rho_e u_e \theta)$  correlation. The correlation constants for proposed correlations 5 and 7, based on the regression analysis applied to the ground-based and flight data, are  $[C_{-95\%}, C, C_{+95\%}] = [25.3, 42.8, 72.5]$  and  $[118.0, 217.6, 401.3]$ , respectively.

### 4.4 Selection of Correlation Constants

As per the down-select process in Section 4.3, the recommended options 1 and 2 for the BLT Tool V.2 protuberance correlations are proposed correlations 5 and 7, respectively. The recommended ensemble correlation plots, which includes both ground-based and flight data, were presented in Figures 16 and 18. For clarity, the recommended correlations are re-plotted in Figures 19 and 20 with only the flight data. Error bars due to uncertainties in protrusion heights,  $k$ , assuming 95% confidence limits for the quoted uncertainties (refer to Table 8), are also presented in the figures (see end of Section 4.1 for details). For both recommended options, the flight data are consistently biased towards the  $C_{+95\%}$  curve. This will result in overly conservative correlations, with respect to the tool's transition predictive capabilities, if the selected best estimate correlation coefficients,  $C$ , are used. A methodology was decided upon by the Aeroheating Panel to derive a new set of correlation coefficients using the entire database. Stated briefly, the best estimate correlation coefficient will be derived from the nominal flight data, and the 95% confidence limits will be based on the extensive ground-based data. It should be noted that the  $k$  values measured on the ground upon landing for the nominal flight cases were assumed to have the same values during reentry, i.e. aerodynamic forces, landing forces, and ablation of the gap-filler material do not appreciably change the height of the protruding gap filler.

The rationale for this methodology, agreed upon by the Aeroheating Panel, can be summarized with the following statements. As is evident from the preceding sections, extensive ground-based measurements have been acquired for a range of Mach numbers and  $k/\delta$  values to examine the effects on transition onset of protuberance geometry, orientation, and spatial location all on the windward surface of sub-scale Orbiter models. The recommended correlations clearly indicate a bias between the *best fit* of the flight data and ground-based data (see Figures 19 and 20). It should be noted, however, that correlations based on the nominal flight data have very similar slope values,  $n$ , as correlations based on the entire ensemble database, i.e. similar correlation trends. Whether these differences should be attributed to the ground test versus the flight environment, uncertainties in the flight protrusion geometries (see discussion in Section 3.5), numerical modeling inconsistency, scaling issues, or some other factor is unclear. For example, the ground-based facilities do not accurately simulate the reentry flight conditions experienced by the Orbiter (e.g., high-temperature effects). Secondly, the ground-based facilities inherently have a noise environment, due to radiation from the turbulent nozzle-wall boundary layers, not realized in flight. Taking into account the aforementioned comments, the decision was made to use the best fit correlation

coefficient derived from the nominal flight data (ten accepted cases) as the best estimate coefficient for the recommended correlations. This removes the unwanted bias between the best estimate coefficients of the correlations and the flight data. The 95% confidence limits are derived using the extensive ground-based data as it includes more protuberance geometry and location effects than the flight data. The confidence limits are derived by equating the ground-based uncertainty to the desired uncertainty about the best estimate coefficient for the respective correlations (details to follow).

#### 4.4.1 Option 1 Correlation (PC#5)

Recall for the option 1 correlation (i.e., proposed correlation 5), the disturbance and transition parameters are  $(k/\delta)(H_e/H_w)^{0.30}$  and  $Re_\theta/M_e$ , respectively, where the slope is  $n = -1$ . Regression analysis was applied to the nominal flight data accepted by the Aeroheating Panel. The analysis results in very good metrics for the correlation. The best fit correlation constant for the accepted flight data is taken to be  $C = C_{\text{fit}} = 61.3$ , where the subscript ‘fit’ denotes flight data. The new 95% confidence limits are derived based on the uncertainty values obtained from the ensemble of the ground-based data. The analysis is easily done in the regression space, i.e.,  $\hat{X}$ - $\hat{Y}$  space (refer back to Section 2.2). For the current correlation approach applied to the ensemble ground-based data, the best fit is  $C_{\text{gb}} = 41.6$ , where the subscript ‘gb’ denotes ensemble ground-based data. Recall from Section 2.2 that  $\hat{C} = \log C$ . The newly derived uncertainty,  $2S_{\hat{Y}}/\hat{C}$ , is equated to the ground-based uncertainty,  $2S_{\hat{Y},\text{gb}}/\hat{C}_{\text{gb}}$ , where  $S_{\hat{Y}}$  is defined in Eq. 7 and  $S_{\hat{Y},\text{gb}} = 0.109$ . The newly derived standard error becomes  $S_{\hat{Y}} = S_{\hat{Y},\text{gb}} \times \hat{C}/\hat{C}_{\text{gb}}$ . The 95% confidence coefficients are then computed using Eqs. 8 and 9. The newly derived coefficients for option 1 correlation are  $(C_{-95\%}, C, C_{+95\%}) = (35.3, 61.3, 106.4)$  versus  $(C_{-95\%}, C, C_{+95\%}) = (25.3, 42.8, 72.5)$  for the total ensemble of ground-based and flight data. Both sets of coefficients are tabulated in Table 12 for convenience.

A plot showing the newly derived correlation coefficients and the flight data with associated error bars, assuming 95% confidence limits for the quoted uncertainties in  $k$ , is presented in Figure 21. In the following plots,  $C$  (“BF Flight”) denotes best fit coefficient for the flight data. It should be noted that the uncertainties in the accepted flight data are all contained within the 95% confidence limits of the correlation. If 68% confidence limits for the quoted uncertainties in  $k$  are assumed, then the errors bars are twice those in Figure 21 due to the linear dependence of the disturbance parameter to  $k$ . For this assumed larger uncertainty band, five of the accepted flight cases can potentially lie below the  $C_{-95\%}$  line, i.e., STS-55 (2 cases), STS-94, STS-99, and STS-103. These flight cases represent the largest quoted  $k$  uncertainties ( $\pm 25\%$  to  $\pm 30\%$ ) and most likely already represent approximate 95% confidence limits ( $\approx \pm 2\sigma$  uncertainty bands) instead of the assumed 68% confidence limits (see discussion at the end of Section 4.1). Figure 22 shows a plot with all the available data and the newly derived correlation curves. The large  $k/\delta$ , Mach 16 data, both laminar and transitional, are indicated in the figure. These data are out of family from the observed correlation trends. As expected, some of the ground-based data lie below the  $C_{-95\%}$  curve. To put this correlation in perspective, the historical flight data with the measured EI transition times are shown in Table 13. Results from one post STS-107 flight, i.e. STS-121, are included at the end of the table as an added flight case. The predicted transition times using the associated flight trajectories for this correlation are shown in the table. The predicted times are based on the correlations coefficients recommended by the Aeroheating Panel (see Table 12). Note the good agreement between the measured transition times and the best estimate (BE) transition times for PC#5 with the recommended coefficients.

#### 4.4.2 Option 2 Correlation (PC#7)

The discussion for the option 2 correlation (i.e., proposed correlation 7) is very similar to the above discourse for the option 1 correlation. The disturbance and transition parameters are  $(\rho_k u_k k)/(\rho_e u_e \theta)$  and  $\rho_e u_e \theta/\mu_k$ , respectively, where the slope is  $n = -0.6$ . The regression analysis applied to the nominal flight data accepted by the Aeroheating Panel resulted in a new best fit correlation constant of  $C = C_{\text{fit}} = 396.8$ . As before, the new 95% confidence limits are derived based on the uncertainty values obtained from the ensemble of the ground-based data. The best fit constant and standard error for the ground-based ensemble data are  $C_{\text{gb}} = 207.5$  and  $S_{\hat{Y},\text{gb}} = 0.114$ , respectively. The newly derived standard error becomes  $S_{\hat{Y}} = S_{\hat{Y},\text{gb}} \times \hat{C}/\hat{C}_{\text{gb}}$ . The 95% confidence coefficients are then computed using Eqs. 8 and 9. The newly derived coefficients for option 2 correlation are  $(C_{-95\%}, C, C_{+95\%}) = (220.7, 396.8, 713.4)$  versus  $(C_{-95\%}, C, C_{+95\%}) = (118.0, 217.6, 401.3)$  for the total ensemble of ground-based and flight data. Both sets of coefficients are tabulated in Table 12 for reference.

A correlation plot utilizing the newly derived coefficients and the flight data with associated error bars is presented in Figure 23. The errors bars in this figure assume 95% confidence limits for the quoted uncertainties in  $k$ . Note that all the uncertainties in the accepted flight data are all contained well within the 95% confidence limits of the correlation. Figure 24 shows a plot with all the available data and the newly derived correlation curves. The large  $k/\delta$ , Mach 16 data, both laminar and transitional, are indicated in the figure. These data points are in the same family with the lower Mach number data and the observed correlation trends. As expected, some of the ground-based data lie below the  $C_{-95\%}$  curve. Table 13 also shows the predicted transition times using this correlation.

#### 4.5 Correlations Revisted

Recall from the analysis in Section 4.2, that improved data collapse in the correlation parameters was obtained with the implementation of a temperature or total enthalpy ratio. Specifically in Section 4.2.3, the inclusion of the total enthalpy ratio in the disturbance parameter,  $X = [(k/\delta)(H_e/H_w)^m]$ , provided improved correlation metrics as compared with  $X = k/\delta$  (compare PC's#1 and #5 in Table 11). A similar procedure using the entire database was conducted during the development of the BLT Tool V.2 for  $X = k/\delta^*$ , but the improvements in the correlation metrics with the addition of these ratios were secondary to the proposed correlation #5. Due to the relative lack of collapse (poor correlation metrics) when correlating with a disturbance parameter,  $X = k/\theta$  (see Table 11), the implementation of the temperature or total enthalpy ratio was not pursued during the development of the BLT Tool V.2. More recently, this was examined for both  $X = [(k/\theta)(T_e/T_w)^m]$  and  $X = [(k/\theta)(H_e/H_w)^m]$  with interesting results for regression exponents of  $n = -1$ . The improvements made in the correlation metrics with the inclusion of the temperature ratio are still not as good as those with PC#5; however, improvements better than PC#5 are observed with the addition of the total enthalpy ratio. The correlation metrics are summarized in Table 14 for the entire database (ground-based + flight data). Note the improvements in the metrics between PC#5 and the total enthalpy ratio implementation of  $X = k/\theta$  (line with right arrow) in the table, albeit small for  $R$  and  $\Delta C/C$ . A 25% improvement in the facility-to-facility variability ( $\sigma_C/\bar{C}$ ) is observed. A plot of this correlation is shown in Figure 25. Two observations with this revised correlation are that the flight data are consistently biased towards the  $C_{+95\%}$  line and that the Mach 16 data for the large  $k/\delta$  are out of family for this correlation, similar to observations made for PC#5. Upon applying the methodology of the Aeroheating Panel as described in Section 4.4, the flight and ground-based data are re-plotted with the newly derived coefficients in Figure 26. The newly derived coefficients for this correlation are  $(C_{-95\%}, C, C_{+95\%}) = (268.0, 450.7, 758.1)$

versus  $(C_{-95\%}, C, C_{+95\%}) = (212.0, 350.3, 578.8)$  for the total ensemble of ground-based and flight data.

## 4.6 Assumptions and Limitations

There are a few key assumptions employed in the development of the proposed BLT correlations that need to be mentioned.

- The main underlying assumption is that the ground-based transition database provides an adequate representation for the flight database. Firstly, the ground-based facilities are incapable of simulating the actual flight conditions experienced during reentry. These include, but are not limited to, high-temperature effects, appropriate freestream Mach number range, and environmental noise conditions. All conventional hypersonic facilities are known to radiate noise from the transitional/turbulent nozzle-wall boundary layers. This radiated noise has been shown to affect transition measurements for a range of transition mechanisms.
- The protuberance heights,  $k$ , used in the sub-scale ground-based tests assume a scaling based on local boundary-layer flow parameters like  $Re_\theta$ ,  $Re_k$ ,  $M_e$ ,  $\delta$ , etc.
- BLT correlations developed with ground-based data and simplified protuberance geometries are assumed directly scaleable to flight.
- The nominal flight data are used to select the recommended best estimate correlation coefficient even with the known geometry uncertainties in flight. Recall that geometry measurements were all acquired upon Shuttle landing. In addition, the possibility of the protuberances (gap fillers) bending or deforming under the aerodynamic loads of reentry are unknown.
- The extensive ground-based data are used to estimate the 95% confidence limits of the recommended correlation coefficients.

With the assumptions above, it should be noted that the historical flight data, for most of the proposed correlations, lie within the 95% confidence limit of the entire database (refer to Sections 4.2 and 4.4 for details).

The limitations of the BLT correlations need to be clearly stated. Caution needs to be exercised to insure that the correlations are applied within the range of parameters used in the development.

- The correlations are applicable on the windward surface of the Orbiter for protuberances inboard of and on the attachment lines.
- The ratio of protuberance height to local boundary-layer thickness is  $0.1 \leq k/\delta \leq 3.5$ . For large  $k/\delta$  and  $M$  values (e.g.,  $k/\delta \geq 1.3$  and  $M \geq 16$ ), preference should be given to PC#7 ( $Re_k$ -type approach) since it collapses the data better than PC#5 ( $Re_\theta/M_e$ -type approach).
- Apply BLT correlations using a consistent computational framework to that utilized during development.

The BLT correlations were developed within a limited parameter range due to restricted range in facilities and available data. As a result, there is no data to validate and/or anchor the correlations outside of the limited parameter range so the end user must be cognizant when exceeding the following bounds.

- The correlations were developed with protuberances located at  $x/L_{ref}$  values in the range of  $0.1 \leq x/L_{ref} \leq 0.85$ .

- The correlations were developed using transition data with freestream Mach numbers in the range of  $6 \leq M_\infty \leq 19$ .

## 5 Summary

Boundary layer transition data specific to the Space Shuttle Orbiter, acquired in four ground-based facilities (LaRC 20-Inch Mach 6 Air Tunnel, LaRC 31-Inch Mach 10 Air Tunnel, LaRC 20-Inch Mach 6 CF<sub>4</sub> Tunnel, and CUBRC LENS-I Shock Tunnel) using three wind tunnel model scales (0.75, 0.90, and 1.8%) plus Orbiter historical flight data, have been analyzed to develop an engineering tool for windward-side Orbiter reentry transition prediction. BLT engineering correlations were presented using a N-S database developed for both ground-based and flight conditions. It was demonstrated that the BLT Tool V.1 applied with the N-S database provided better data collapse than with the LATCH database. In all the regression analysis, the large  $k/\delta$  ( $> 1.3$ ) data at Mach 16 were not included in the analysis and are excluded from the correlation metrics. Of the correlation tools examined during the development of the BLT Tool V.2, the proposed correlation 5 with  $X = (k/\delta) \times (H_e/H_w)^{0.30}$  and  $Y = Re_\theta/Me$  was found to provide the best overall correlation metrics when the entire database of ground-based and flight data is employed. The large  $k/\delta$ , Mach 16 data were out of family for this correlation. The second independent correlation (proposed correlation 7) selected uses  $X = (\rho_k u_k k)/(\rho_e u_e \theta)$  and  $Y = \rho_e u_e \theta / \mu_k$  as the disturbance and transition parameters, respectively. This correlation, developed using the entire ground-based and flight database, provided an overall data collapse to include the Mach 16, large  $k/\delta$  data, but the metrics were not as good as proposed correlation 5. The Aeroheating Panel adopted an approach to select the recommended correlation coefficients for version 2 of the protuberance BLT Tool. The coefficients for the BLT Tool V.2 are summarized in Table 12. The BLT Tool V.2 has been baselined and approved by the Orbiter Project Office in the Space Shuttle Program as part of the transition prediction tool for use by the Damage Assessment Team for real-time evaluation of the Orbiter's TPS prior to reentry. The protuberance correlations were recently revisited and an improved correlation with  $X = (k/\theta) \times (H_e/H_w)^{0.44}$  and  $Y = Re_\theta/Me$  was obtained. The improved metrics are marginally superior and have similar trends to the proposed correlation 5. Consequently, there is not a strong justification for re-baselining of the protuberance correlation for the BLT Tool V.2.

## References

1. Campbell, C. H., Anderson, B., Bourland, G., Bouslog, S., Cassady, A., Horvath, T. J., Berry, S. A., Gnoffo, P. A., Wood, W. A., Reuther, J. J., Driver, D. M., Chao, D. C., Hyatt, J., and Picetti, D., "Orbiter Return To Flight Entry Aeroheating," AIAA Paper 2006-2917, June 2006.
2. Berry, S. A., Horvath, T.J., Greene, F. A., Kinder, G. R., and Wang, K. C., "Overview of Boundary Layer Transition Research in Support of Orbiter Return To Flight," AIAA Paper 2006-2918, June 2006.
3. Horvath, T. J., Berry, S. A., Merski, N. R., Berger, K. T., Buck, G. M., Liechty, D. S., and Schneider, S. P., "Shuttle Damage/Repair from the Perspective of Hypersonic Boundary Layer Transition – Experimental Results," AIAA Paper 2006-2919, June 2006.
4. Greene, F. A., and Hamilton, H. H., "Development of a Boundary Layer Properties Interpolation Tool in Support of Orbiter Return to Flight," AIAA Paper 2006-2920, June 2006.
5. McGinley, C. B., Berry, S. A., Kinder, G. R., Barnwell, M., Wang, K. C., and Kirk, S. K., "Review of Orbiter Flight Boundary Layer Transition Data," AIAA Paper 2006-2921, June 2006.
6. Berry, S. A., Horvath, T.J., Cassady, A. M., Kirk, B. S., Wang, K. C., and Hyatt, A. J., "Boundary Layer Transition Results From STS-114," AIAA Paper 2006-2922, June 2006.
7. Kegerise, M. A., King, R. A., and Berry, S. A., "Development of Cavity Induced Boundary-Layer Transition Correlations for Version 2.0 of the BLT Tool," Engineering Note EG-SS-07-05, NASA Johnson Space Center, March 2007.
8. Hamilton, H. H., II, Greene, F. A., and DeJarnette, F. R., "Approximate Method for Calculating Heating Rates on Three-Dimensional Vehicles," *Journal of Spacecraft and Rockets*, Vol. 31, No. 3, 1994, pp. 345-354.
9. Gnoffo, P. A., "An Upwind-Biased, Point-Implicit Algorithm for Viscous, Compressible Perfect Gas Flows," NASA TP-2953, 1990.
10. Wright, M. J., Candler, G. V., and Bose, D., "Data-Parallel Line Relaxation Method for the Navier-Stokes Equations," *AIAA Journal*, Vol. 36, No. 9, 1998, pp. 1603-1609.
11. Meyer, B., "A Boundary Layer Probing and Reynolds Number Interpolation Tool: Blvolprops v3.0," Swales Technical Note 06-488, Hypersonic Vehicle Analysis Group, NASA Langley Research Center, November 2006.
12. Wood, W. A., Alter, S. J., Greene, F. A., Driver, D. M., Prabhu, R. K., Meyer, B., Saunders, D. K., Mazaheri, A., and Calloway, R. L., "Viscous-CFD Space Shuttle Orbiter Boundary Layer Data and Probe Software," Engineering Note EG-SS-07-10, NASA Johnson Space Center, March 2007.
13. Berkowitz, A. M., Kyriss, C. L., and Martellucci, A., "Boundary Layer Transition Flight Test Observations," AIAA Paper 1977-125, January 1977.

14. Reda, D. C., "Review and Synthesis of Roughness-Dominated Transition Correlations for Reentry Applications," *Journal of Spacecraft and Rockets*, Vol. 39, No. 2, 2002, pp. 161-167.
15. Coleman, H. W. and Steele, W. G., "Experimentation and Uncertainty Analysis for Engineers—2nd Edition," John Wiley & Sons, Inc., 1999.
16. Rhode, M. N., and DeLoach, R., "Hypersonic Wind Tunnel Calibration Using the Modern Design of Experiments," AIAA Paper 2005-4274, July 2005.
17. Holden, M. S., Wadhams, T. P., Harvey, J. K., and Candler, G. V., "Comparisons Between DSMC and Navier-Stokes Solutions and Measurements in Regions of Laminar Shock Wave Boundary Layer Interaction in Hypersonic Flows," AIAA Paper 2002-0435, January 2002.
18. Miller, C. G., "Hypersonic Aerodynamic/Aerthermodynamic Testing Capabilities at Langley Research Center," AIAA Paper 1992-3937, July 1992.
19. AAEC Research Staff, LENS Brochure, *Capabilities and Technologies*, Buffalo, NY 2004.
20. Liechty, D. S., Berry, S. A., and Horvath, T. J., "Shuttle Return To Flight Experimental Results: Protuberance Effects on Boundary Layer Transition," NASA TM-2006-214306, June 2006.
21. Kegerise, M. A., King, R. A., and Berry, S. A., "Wind Tunnel Test in Support of STS-121: Protuberance Effects on Boundary-Layer Transition," Engineering Note EG-SS-07-06, NASA Johnson Space Center, March 2007.
22. King, R. A., Berry, S. A., and Kegerise, M. A., "Effect of Protuberance Shape and Orientation on Space Shuttle Orbiter Boundary-Layer Transition," NASA TM-2008-215103, February 2008.
23. Micol, J. R., Midden, R. E., and Miller, C. G., "Langley 20-Inch Hypersonic CF<sub>4</sub> Tunnel: A Facility for Simulating Real-Gas Effects," AIAA Paper 1992-3939, July 1992.
24. Cassady, A. M., Bourland, G., King, R. A., Kegerise, M. A., Marichalar, J., Kirk, B. S., and Treviño, L., "MH-13 Space Shuttle Orbiter Aerothermodynamic Test Report," NASA TP-2007-214758, 2007.
25. Wadhams, T. P., Smolinski, G. J., Holden, M. S., and MacLean, M. G., "Experimental Space Shuttle Orbiter Studies to Acquire Data for Code and Flight Heating Model Validation," AIAA Paper 2007-551, January 2007.
26. McGinley, C. B., Berry, S. A., "Orbiter Historical Flight Boundary Layer Transition," Engineering Note EG-SS-07-09, NASA Johnson Space Center, March 2007.
27. Wood, W. A., Erickson, D. W., and Greene, F. A., "Orbiter Entry Aeroheating Working Group viscous CFD boundary layer transition trailblazer solutions," NASA TM-2007-214882, June 2007.
28. Bouslog, S. A., Bertin, J. J., Berry, S. A., and Caram, J. M., "Isolated Roughness Induced Boundary-Layer Transition – Shuttle Orbiter Ground Tests And Flight Experience," AIAA Paper 1997-0274, January 1997.

Table 1. Relevant correlation parameters derived from the N-S database at the estimated unit  $Re_{\infty,inc}$  values for data obtained in the NASA LaRC 20-Inch Mach 6 Tunnel.

| $x/L_{ref}$ | $y/L_{ref}$ | $Re_{\infty}/ft$<br>( $1 \times 10^6$ ) | $k$ (in.) | $M_e$ | $Re_{\theta}/M_e$ | $\delta$ (in.) | $\delta^*$ (in.) | $\theta$ (in.) | $H_e/H_w$ | $T_e/T_w$ | $\rho_e u_e$<br>(lb-s/ft <sup>3</sup> ) | $\rho_e u_k$<br>(lb-s/ft <sup>3</sup> ) | $\mu_k$<br>(lb-s/ft <sup>2</sup> ) | $\mu_w$<br>(lb-s/ft <sup>2</sup> ) |
|-------------|-------------|---|-----------|-------|-------------------|----------------|------------------|----------------|-----------|-----------|---|---|------------------------------------|------------------------------------|
| 0.10        | 0.0000      | 2.2500                                  | 0.0045    | 1.07  | 96.60             | 0.0114         | 0.0030           | 0.0016         | 1.68      | 1.37      | 0.3868                                  | 0.2916                                  | 4.67e-07                           | 3.86e-07                           |
| 0.10        | 0.0134      | 2.2500                                  | 0.0045    | 1.08  | 92.20             | 0.0109         | 0.0029           | 0.0015         | 1.68      | 1.36      | 0.3903                                  | 0.3011                                  | 4.68e-07                           | 3.86e-07                           |
| 0.30        | 0.0000      | 1.8850                                  | 0.0065    | 1.39  | 120.00            | 0.0170         | 0.0058           | 0.0023         | 1.68      | 1.21      | 0.3833                                  | 0.2322                                  | 4.50e-07                           | 3.86e-07                           |
| 0.30        | 0.0454      | 1.8850                                  | 0.0065    | 1.45  | 104.00            | 0.0151         | 0.0053           | 0.0021         | 1.68      | 1.18      | 0.3879                                  | 0.2518                                  | 4.48e-07                           | 3.86e-07                           |
| 0.40        | 0.0000      | 1.5500                                  | 0.0065    | 1.47  | 120.00            | 0.0195         | 0.0070           | 0.0027         | 1.68      | 1.18      | 0.3459                                  | 0.1788                                  | 4.44e-07                           | 3.86e-07                           |
| 0.40        | 0.0706      | 1.8750                                  | 0.0065    | 1.53  | 108.00            | 0.0149         | 0.0054           | 0.0020         | 1.68      | 1.15      | 0.4208                                  | 0.2661                                  | 4.44e-07                           | 3.86e-07                           |
| 0.50        | 0.0000      | 2.2800                                  | 0.0045    | 1.49  | 161.00            | 0.0174         | 0.0064           | 0.0024         | 1.68      | 1.17      | 0.5180                                  | 0.2175                                  | 4.36e-07                           | 3.86e-07                           |
| 0.50        | 0.1008      | 1.8950                                  | 0.0045    | 1.58  | 118.00            | 0.0151         | 0.0057           | 0.0020         | 1.68      | 1.12      | 0.4650                                  | 0.2089                                  | 4.38e-07                           | 3.86e-07                           |
| 0.50        | 0.0000      | 1.2050                                  | 0.0065    | 1.54  | 117.00            | 0.0233         | 0.0087           | 0.0032         | 1.68      | 1.14      | 0.2896                                  | 0.1242                                  | 4.36e-07                           | 3.86e-07                           |
| 0.50        | 0.1008      | 1.9100                                  | 0.0065    | 1.58  | 119.00            | 0.0151         | 0.0057           | 0.0020         | 1.68      | 1.12      | 0.4688                                  | 0.2826                                  | 4.43e-07                           | 3.86e-07                           |
| 0.60        | 0.0000      | 1.8800                                  | 0.0045    | 1.55  | 162.00            | 0.0205         | 0.0078           | 0.0028         | 1.68      | 1.14      | 0.4551                                  | 0.1563                                  | 4.29e-07                           | 3.86e-07                           |
| 0.60        | 0.1429      | 1.8800                                  | 0.0045    | 1.72  | 75.00             | 0.0098         | 0.0036           | 0.0013         | 1.69      | 1.06      | 0.4925                                  | 0.3184                                  | 4.31e-07                           | 3.86e-07                           |
| 0.60        | 0.0000      | 0.9500                                  | 0.0115    | 1.60  | 115.00            | 0.0281         | 0.0108           | 0.0038         | 1.68      | 1.12      | 0.2452                                  | 0.1381                                  | 4.40e-07                           | 3.86e-07                           |
| 0.60        | 0.1429      | 1.2400                                  | 0.0065    | 1.75  | 61.40             | 0.0120         | 0.0044           | 0.0015         | 1.69      | 1.05      | 0.3353                                  | 0.2410                                  | 4.26e-07                           | 3.86e-07                           |
| 0.64        | 0.0000      | 1.4400                                  | 0.0065    | 1.58  | 150.00            | 0.0242         | 0.0094           | 0.0033         | 1.68      | 1.12      | 0.3649                                  | 0.1448                                  | 4.33e-07                           | 3.86e-07                           |
| 0.64        | 0.1701      | 1.4400                                  | 0.0045    | 1.75  | 36.70             | 0.0054         | 0.0021           | 0.0007         | 1.68      | 1.04      | 0.4328                                  | 0.3985                                  | 4.08e-07                           | 3.87e-07                           |
| 0.64        | 0.0000      | 0.9650                                  | 0.0115    | 1.61  | 123.00            | 0.0290         | 0.0114           | 0.0039         | 1.68      | 1.11      | 0.2522                                  | 0.1355                                  | 4.39e-07                           | 3.86e-07                           |
| 0.64        | 0.1701      | 0.7050                                  | 0.0115    | 1.78  | 25.30             | 0.0074         | 0.0030           | 0.0010         | 1.65      | 1.01      | 0.2185                                  | 0.2422                                  | 3.74e-07                           | 3.87e-07                           |
| 0.66        | 0.0000      | 2.6750                                  | 0.0045    | 1.54  | 213.00            | 0.0188         | 0.0072           | 0.0026         | 1.69      | 1.15      | 0.6525                                  | 0.2398                                  | 4.32e-07                           | 3.86e-07                           |
| 0.66        | 0.1908      | 1.5300                                  | 0.0035    | 1.94  | 24.90             | 0.0037         | 0.0013           | 0.0004         | 1.67      | 0.95      | 0.5227                                  | 0.5104                                  | 3.76e-07                           | 3.87e-07                           |
| 0.68        | 0.0000      | 1.8750                                  | 0.0045    | 1.57  | 181.00            | 0.0223         | 0.0086           | 0.0031         | 1.68      | 1.13      | 0.4738                                  | 0.1465                                  | 4.26e-07                           | 3.86e-07                           |
| 0.68        | 0.2111      | 1.2150                                  | 0.0045    | 1.83  | 23.00             | 0.0034         | 0.0013           | 0.0004         | 1.67      | 1.00      | 0.4671                                  | 0.4811                                  | 3.84e-07                           | 3.87e-07                           |
| 0.20        | 0.0000      | 1.9150                                  | 0.0065    | 1.68  | 93.70             | 0.0191         | 0.0067           | 0.0024         | 1.68      | 1.08      | 0.3145                                  | 0.1684                                  | 4.27e-07                           | 3.86e-07                           |
| 0.20        | 0.0370      | 1.9150                                  | 0.0065    | 1.73  | 76.40             | 0.0155         | 0.0056           | 0.0020         | 1.68      | 1.05      | 0.3220                                  | 0.1983                                  | 4.26e-07                           | 3.86e-07                           |
| 0.40        | 0.0000      | 1.8400                                  | 0.0065    | 1.82  | 114.00            | 0.0217         | 0.0090           | 0.0028         | 1.68      | 1.01      | 0.3491                                  | 0.1374                                  | 4.28e-07                           | 3.86e-07                           |
| 0.40        | 0.0824      | 1.8400                                  | 0.0065    | 1.95  | 84.20             | 0.0157         | 0.0067           | 0.0020         | 1.68      | 0.96      | 0.3737                                  | 0.1875                                  | 4.24e-07                           | 3.86e-07                           |
| 0.60        | 0.0000      | 2.2550                                  | 0.0065    | 1.90  | 161.00            | 0.0231         | 0.0101           | 0.0029         | 1.68      | 0.98      | 0.4731                                  | 0.1648                                  | 4.25e-07                           | 3.86e-07                           |
| 0.60        | 0.1462      | 1.8950                                  | 0.0065    | 2.15  | 49.50             | 0.0076         | 0.0034           | 0.0009         | 1.69      | 0.88      | 0.4890                                  | 0.4404                                  | 3.65e-07                           | 3.86e-07                           |
| 0.64        | 0.0000      | 2.7400                                  | 0.0065    | 1.90  | 188.00            | 0.0221         | 0.0097           | 0.0028         | 1.69      | 0.98      | 0.5785                                  | 0.2073                                  | 4.26e-07                           | 3.86e-07                           |
| 0.64        | 0.1754      | 1.5650                                  | 0.0045    | 2.57  | 20.10             | 0.0036         | 0.0015           | 0.0003         | 1.67      | 0.72      | 0.5724                                  | 0.6076                                  | 2.91e-07                           | 3.88e-07                           |

$L_{ref} = 9.6$  in

Table 1. Relevant correlation parameters derived from the N-S database at the estimated unit  $Re_{\infty,inc}$  values for data obtained in the NASA LaRC 20-Inch Mach 6 Tunnel – (Cont).

| $x/L_{ref}$ | $y/L_{ref}$ | $Re_{\infty}/ft$<br>( $1 \times 10^6$ ) | $k$ (in.) | $M_e$ | $Re_{\theta}/M_e$ | $\delta$ (in.) | $\delta^*$ (in.) | $\theta$ (in.) | $H_e/H_w$ | $T_e/T_w$ | $\rho_e u_e$<br>(lb-s/ft <sup>3</sup> ) | $\rho_k u_k$<br>(lb-s/ft <sup>3</sup> ) | $\mu_k$<br>(lb-s/ft <sup>2</sup> ) | $\mu_w$<br>(lb-s/ft <sup>2</sup> ) |
|-------------|-------------|---|-----------|-------|-------------------|----------------|------------------|----------------|-----------|-----------|---|---|------------------------------------|------------------------------------|
| 0.30        | 0.0000      | 1.5550                                  | 0.0045    | 1.41  | 109.00            | 0.0186         | 0.0064           | 0.0025         | 1.68      | 1.21      | 0.3204                                  | 0.1356                                  | 4.37e-07                           | 3.86e-07                           |
| 0.30        | 0.0236      | 1.5550                                  | 0.0045    | 1.42  | 105.00            | 0.0179         | 0.0062           | 0.0024         | 1.68      | 1.20      | 0.3240                                  | 0.1398                                  | 4.38e-07                           | 3.86e-07                           |
| 0.40        | 0.0000      | 1.7500                                  | 0.0045    | 1.46  | 128.00            | 0.0184         | 0.0066           | 0.0025         | 1.68      | 1.18      | 0.3856                                  | 0.1555                                  | 4.36e-07                           | 3.86e-07                           |
| 0.40        | 0.0504      | 1.7500                                  | 0.0045    | 1.49  | 115.00            | 0.0167         | 0.0060           | 0.0023         | 1.68      | 1.16      | 0.3920                                  | 0.1715                                  | 4.37e-07                           | 3.86e-07                           |
| 0.50        | 0.0000      | 1.2500                                  | 0.0045    | 1.53  | 119.00            | 0.0229         | 0.0086           | 0.0031         | 1.68      | 1.15      | 0.3008                                  | 0.0960                                  | 4.27e-07                           | 3.86e-07                           |
| 0.50        | 0.0874      | 1.7500                                  | 0.0045    | 1.56  | 121.00            | 0.0168         | 0.0064           | 0.0023         | 1.68      | 1.13      | 0.4265                                  | 0.1720                                  | 4.35e-07                           | 3.86e-07                           |
| 0.60        | 0.0000      | 1.7500                                  | 0.0045    | 1.55  | 156.00            | 0.0212         | 0.0081           | 0.0029         | 1.68      | 1.14      | 0.4272                                  | 0.1422                                  | 4.28e-07                           | 3.86e-07                           |
| 0.60        | 0.1311      | 1.2450                                  | 0.0045    | 1.66  | 80.10             | 0.0147         | 0.0055           | 0.0019         | 1.68      | 1.09      | 0.3437                                  | 0.1575                                  | 4.35e-07                           | 3.86e-07                           |
| 0.70        | 0.0000      | 1.5900                                  | 0.0045    | 1.59  | 169.00            | 0.0244         | 0.0095           | 0.0033         | 1.68      | 1.12      | 0.4071                                  | 0.1176                                  | 4.23e-07                           | 3.86e-07                           |
| 0.70        | 0.2298      | 0.8050                                  | 0.0045    | 1.76  | 19.80             | 0.0041         | 0.0015           | 0.0005         | 1.67      | 1.03      | 0.3224                                  | 0.3276                                  | 3.94e-07                           | 3.87e-07                           |

$L_{ref} = 9.6$  in

Table 2. Relevant correlation parameters derived from the N-S database at the estimated unit  $Re_{\infty,inc}$  values for STS-121 mission support data obtained in the NASA LaRC 20-Inch Mach 6 Air Tunnel.

| $x/L_{ref}$ | $y/L_{ref}$ | $Re_{\infty}/ft$<br>( $1 \times 10^6$ ) | $k$ (in.) | $M_e$ | $Re_{\theta}/M_e$ | $\delta$ (in.) | $\delta^*$ (in.) | $\theta$ (in.) | $H_e/H_w$ | $T_e/T_w$ | $\rho_e u_e$<br>(lb-s/ft <sup>3</sup> ) | $\rho_k u_k$<br>(lb-s/ft <sup>3</sup> ) | $\mu_k$<br>(lb-s/ft <sup>2</sup> ) | $\mu_w$<br>(lb-s/ft <sup>2</sup> ) |
|-------------|-------------|---|-----------|-------|-------------------|----------------|------------------|----------------|-----------|-----------|---|---|------------------------------------|------------------------------------|
| 0.8305      | 0.0530      | 1.7500                                  | 0.0045    | 1.68  | 184.00            | 0.0249         | 0.0092           | 0.0033         | 1.68      | 1.08      | 0.4588                                  | 0.1439                                  | 4.20e-07                           | 3.86e-07                           |
| 0.8305      | 0.0530      | 1.7100                                  | 0.0065    | 1.68  | 182.00            | 0.0251         | 0.0093           | 0.0033         | 1.68      | 1.08      | 0.4511                                  | 0.1862                                  | 4.27e-07                           | 3.86e-07                           |
| 0.8305      | 0.0530      | 0.8200                                  | 0.0115    | 1.73  | 126.00            | 0.0352         | 0.0133           | 0.0046         | 1.69      | 1.05      | 0.2269                                  | 0.1116                                  | 4.29e-07                           | 3.86e-07                           |
| 0.8013      | -0.2747     | 0.9500                                  | 0.0065    | 1.84  | 65.80             | 0.0123         | 0.0048           | 0.0015         | 1.69      | 1.01      | 0.3645                                  | 0.2443                                  | 4.16e-07                           | 3.86e-07                           |

$L_{ref} = 9.6$  in

Table 3. Relevant correlation parameters derived from the N-S database at the estimated unit  $Re_{\infty,inc}$  values for the new data obtained in the NASA LaRC 20-Inch Mach 6 Air Tunnel.

| $x/L_{ref}$ | $y/L_{ref}$ | $Re_{\infty}/ft$<br>( $\times 10^6$ ) | $k$ (in.) | $M_e$ | $Re_{\theta}/M_e$ | $\delta$ (in.) | $\delta^*$ (in.) | $\theta$ (in.) | $H_e/H_w$ | $T_e/T_w$ | $\rho_e \nu_e$<br>(lb-s/ft <sup>3</sup> ) | $\rho_k \nu_k$<br>(lb-s/ft <sup>3</sup> ) | $\mu_k$<br>(lb-s/ft <sup>2</sup> ) | $\mu_w$<br>(lb-s/ft <sup>2</sup> ) |
|-------------|-------------|---------------------------------------|-----------|-------|-------------------|----------------|------------------|----------------|-----------|-----------|---|---|------------------------------------|------------------------------------|
| 0.10        | 0.0000      | 0.9750                                | 0.0080    | 1.11  | 70.20             | 0.0182         | 0.0051           | 0.0025         | 1.68      | 1.35      | 0.1787                                    | 0.1369                                    | 4.68e-07                           | 3.86e-07                           |
| 0.10        | 0.0000      | 0.6850                                | 0.0080    | 1.13  | 59.00             | 0.0213         | 0.0061           | 0.0030         | 1.66      | 1.32      | 0.1276                                    | 0.0881                                    | 4.57e-07                           | 3.86e-07                           |
| 0.50        | 0.0000      | 1.5700                                | 0.0080    | 1.52  | 146.00            | 0.0226         | 0.0084           | 0.0031         | 1.68      | 1.15      | 0.3702                                    | 0.1949                                    | 4.42e-07                           | 3.86e-07                           |
| 0.50        | 0.0000      | 1.1350                                | 0.0070    | 1.54  | 124.00            | 0.0262         | 0.0098           | 0.0036         | 1.68      | 1.14      | 0.2745                                    | 0.1129                                    | 4.35e-07                           | 3.86e-07                           |
| 0.50        | 0.0000      | 1.6450                                | 0.0070    | 1.51  | 150.00            | 0.0222         | 0.0082           | 0.0030         | 1.68      | 1.16      | 0.3869                                    | 0.1857                                    | 4.40e-07                           | 3.86e-07                           |
| 0.70        | 0.0000      | 0.9450                                | 0.0070    | 1.63  | 142.00            | 0.0337         | 0.0132           | 0.0046         | 1.68      | 1.10      | 0.2516                                    | 0.0788                                    | 4.25e-07                           | 3.86e-07                           |
| 0.70        | -0.1658     | 0.7650                                | 0.0080    | 1.78  | 80.00             | 0.0222         | 0.0089           | 0.0029         | 1.68      | 1.02      | 0.2354                                    | 0.1128                                    | 4.27e-07                           | 3.86e-07                           |
| 0.70        | 0.1658      | 1.6450                                | 0.0070    | 1.75  | 117.00            | 0.0155         | 0.0062           | 0.0020         | 1.69      | 1.05      | 0.4839                                    | 0.2856                                    | 4.30e-07                           | 3.86e-07                           |
| 0.70        | 0.0000      | 1.1450                                | 0.0070    | 1.62  | 156.00            | 0.0309         | 0.0121           | 0.0042         | 1.68      | 1.11      | 0.3008                                    | 0.1014                                    | 4.28e-07                           | 3.86e-07                           |
| 0.70        | -0.1658     | 0.9550                                | 0.0080    | 1.78  | 89.10             | 0.0200         | 0.0080           | 0.0026         | 1.69      | 1.03      | 0.2911                                    | 0.1538                                    | 4.29e-07                           | 3.86e-07                           |
| 0.70        | 0.1658      | 1.3650                                | 0.0060    | 1.75  | 107.00            | 0.0169         | 0.0067           | 0.0022         | 1.69      | 1.04      | 0.4063                                    | 0.1958                                    | 4.30e-07                           | 3.86e-07                           |
| 0.70        | 0.0000      | 2.3950                                | 0.0070    | 1.56  | 228.00            | 0.0222         | 0.0085           | 0.0030         | 1.68      | 1.13      | 0.5967                                    | 0.2767                                    | 4.38e-07                           | 3.86e-07                           |
| 0.70        | -0.1658     | 0.9700                                | 0.0080    | 1.78  | 89.80             | 0.0198         | 0.0079           | 0.0026         | 1.69      | 1.04      | 0.2952                                    | 0.1551                                    | 4.29e-07                           | 3.86e-07                           |
| 0.85        | 0.0000      | 0.9900                                | 0.0110    | 1.75  | 142.00            | 0.0351         | 0.0127           | 0.0046         | 1.68      | 1.04      | 0.2604                                    | 0.1299                                    | 4.24e-07                           | 3.86e-07                           |
| 0.85        | 0.0000      | 1.6400                                | 0.0100    | 1.72  | 182.00            | 0.0278         | 0.0099           | 0.0036         | 1.68      | 1.06      | 0.4162                                    | 0.2350                                    | 4.26e-07                           | 3.86e-07                           |
| 0.85        | 0.0000      | 1.3700                                | 0.0100    | 1.73  | 167.00            | 0.0303         | 0.0108           | 0.0040         | 1.69      | 1.05      | 0.3533                                    | 0.1872                                    | 4.25e-07                           | 3.86e-07                           |
| 0.74        | 0.0000      | 1.0000                                | 0.0110    | 1.64  | 149.00            | 0.0334         | 0.0131           | 0.0045         | 1.68      | 1.09      | 0.2686                                    | 0.1249                                    | 4.35e-07                           | 3.86e-07                           |
| 0.74        | -0.2348     | 0.5050                                | 0.0070    | 1.78  | 45.90             | 0.0153         | 0.0059           | 0.0019         | 1.63      | 1.00      | 0.1952                                    | 0.1179                                    | 4.15e-07                           | 3.86e-07                           |
| 0.74        | 0.2348      | 0.6650                                | 0.0080    | 1.79  | 52.40             | 0.0135         | 0.0051           | 0.0017         | 1.66      | 1.01      | 0.2595                                    | 0.1931                                    | 4.11e-07                           | 3.86e-07                           |
| 0.74        | 0.0000      | 1.0000                                | 0.0100    | 1.64  | 149.00            | 0.0334         | 0.0131           | 0.0045         | 1.68      | 1.09      | 0.2686                                    | 0.1148                                    | 4.38e-07                           | 3.86e-07                           |
| 0.74        | -0.2348     | 0.8600                                | 0.0070    | 1.81  | 59.40             | 0.0120         | 0.0045           | 0.0015         | 1.69      | 1.02      | 0.3374                                    | 0.2576                                    | 4.13e-07                           | 3.86e-07                           |
| 0.74        | 0.2348      | 1.3600                                | 0.0060    | 1.81  | 74.50             | 0.0096         | 0.0036           | 0.0012         | 1.68      | 1.02      | 0.5274                                    | 0.4233                                    | 4.10e-07                           | 3.86e-07                           |

$L_{ref} = 11.52$  in

Table 4. Relevant correlation parameters derived from the N-S database at the estimated unit  $Re_{\infty,inc}$  values for data obtained in the NASA LaRC 31-Inch Mach 10 Air Tunnel.

| $x/L_{ref}$ | $y/L_{ref}$ | $Re_{\infty}/ft$<br>( $\times 10^6$ ) | $k$ (in.) | $M_e$ | $Re_{\theta}/M_e$ | $\delta$ (in.) | $\delta^*$ (in.) | $\theta$ (in.) | $H_e/H_w$ | $T_e/T_w$ | $\rho_e v_e$<br>(lb-s/ft <sup>3</sup> ) | $\rho_k v_k$<br>(lb-s/ft <sup>3</sup> ) | $\mu_k$<br>(lb-s/ft <sup>2</sup> ) | $\mu_w$<br>(lb-s/ft <sup>2</sup> ) |
|-------------|-------------|---------------------------------------|-----------|-------|-------------------|----------------|------------------|----------------|-----------|-----------|---|---|------------------------------------|------------------------------------|
| 0.20        | 0.0000      | 1.3550                                | 0.0115    | 1.49  | 71.60             | 0.0234         | 0.0053           | 0.0036         | 3.42      | 2.36      | 0.2487                                  | 0.2108                                  | 6.83e-07                           | 3.87e-07                           |
| 0.20        | 0.0269      | 1.2050                                | 0.0115    | 1.53  | 62.10             | 0.0228         | 0.0052           | 0.0035         | 3.40      | 2.32      | 0.2280                                  | 0.1948                                  | 6.81e-07                           | 3.87e-07                           |
| 0.30        | 0.0000      | 0.9400                                | 0.0115    | 1.63  | 67.40             | 0.0291         | 0.0076           | 0.0044         | 3.40      | 2.23      | 0.2010                                  | 0.1475                                  | 6.49e-07                           | 3.87e-07                           |
| 0.30        | 0.0454      | 0.9400                                | 0.0115    | 1.70  | 59.30             | 0.0263         | 0.0069           | 0.0039         | 3.40      | 2.15      | 0.2040                                  | 0.1554                                  | 6.49e-07                           | 3.87e-07                           |
| 0.40        | 0.0000      | 1.9600                                | 0.0065    | 1.64  | 106.00            | 0.0221         | 0.0059           | 0.0034         | 3.43      | 2.23      | 0.4173                                  | 0.2687                                  | 6.24e-07                           | 3.87e-07                           |
| 0.40        | 0.0706      | 1.6300                                | 0.0065    | 1.75  | 80.70             | 0.0205         | 0.0055           | 0.0030         | 3.42      | 2.12      | 0.3669                                  | 0.2399                                  | 6.20e-07                           | 3.87e-07                           |
| 0.40        | 0.0000      | 0.8250                                | 0.0115    | 1.72  | 69.20             | 0.0322         | 0.0089           | 0.0049         | 3.40      | 2.14      | 0.1950                                  | 0.1316                                  | 6.29e-07                           | 3.87e-07                           |
| 0.40        | 0.0706      | 1.1250                                | 0.0115    | 1.78  | 68.10             | 0.0243         | 0.0066           | 0.0036         | 3.40      | 2.08      | 0.2655                                  | 0.2085                                  | 6.48e-07                           | 3.87e-07                           |
| 0.50        | 0.0000      | 0.9400                                | 0.0115    | 1.78  | 81.40             | 0.0323         | 0.0091           | 0.0049         | 3.40      | 2.08      | 0.2335                                  | 0.1556                                  | 6.23e-07                           | 3.87e-07                           |
| 0.50        | 0.1008      | 1.2100                                | 0.0115    | 1.84  | 76.50             | 0.0239         | 0.0067           | 0.0034         | 3.40      | 2.03      | 0.3128                                  | 0.2427                                  | 6.42e-07                           | 3.87e-07                           |
| 0.60        | 0.0000      | 1.6250                                | 0.0065    | 1.79  | 116.00            | 0.0272         | 0.0077           | 0.0041         | 3.43      | 2.08      | 0.3983                                  | 0.2163                                  | 5.85e-07                           | 3.87e-07                           |
| 0.60        | 0.1429      | 1.2600                                | 0.0065    | 2.00  | 50.70             | 0.0153         | 0.0042           | 0.0021         | 3.41      | 1.89      | 0.3528                                  | 0.2586                                  | 6.17e-07                           | 3.88e-07                           |
| 0.60        | 0.0000      | 0.9550                                | 0.0115    | 1.83  | 90.10             | 0.0344         | 0.0099           | 0.0051         | 3.40      | 2.05      | 0.2485                                  | 0.1584                                  | 6.12e-07                           | 3.87e-07                           |
| 0.60        | 0.1429      | 1.1300                                | 0.0115    | 2.00  | 48.40             | 0.0161         | 0.0045           | 0.0022         | 3.41      | 1.89      | 0.3191                                  | 0.2923                                  | 6.22e-07                           | 3.88e-07                           |
| 0.70        | 0.0000      | 0.9500                                | 0.0115    | 1.88  | 101.00            | 0.0374         | 0.0111           | 0.0055         | 3.40      | 1.99      | 0.2600                                  | 0.1548                                  | 6.00e-07                           | 3.87e-07                           |
| 0.70        | 0.2298      | 0.9500                                | 0.0115    | 1.97  | 17.90             | 0.0055         | 0.0012           | 0.0007         | 3.35      | 1.89      | 0.3921                                  | 0.3993                                  | 6.12e-07                           | 3.92e-07                           |
| 0.20        | 0.0000      | 1.6150                                | 0.0115    | 1.92  | 67.20             | 0.0260         | 0.0072           | 0.0038         | 3.42      | 1.97      | 0.2566                                  | 0.1934                                  | 6.20e-07                           | 3.87e-07                           |
| 0.20        | 0.0370      | 1.3550                                | 0.0115    | 2.01  | 51.80             | 0.0236         | 0.0067           | 0.0033         | 3.40      | 1.88      | 0.2307                                  | 0.1787                                  | 6.16e-07                           | 3.88e-07                           |
| 0.30        | 0.0000      | 1.6250                                | 0.0115    | 2.05  | 76.30             | 0.0279         | 0.0088           | 0.0040         | 3.43      | 1.86      | 0.2852                                  | 0.1917                                  | 6.11e-07                           | 3.87e-07                           |
| 0.30        | 0.0571      | 1.3550                                | 0.0115    | 2.21  | 55.70             | 0.0242         | 0.0080           | 0.0033         | 3.40      | 1.73      | 0.2568                                  | 0.1797                                  | 5.99e-07                           | 3.87e-07                           |
| 0.40        | 0.0000      | 1.6200                                | 0.0115    | 2.14  | 84.60             | 0.0287         | 0.0097           | 0.0040         | 3.43      | 1.79      | 0.3182                                  | 0.1986                                  | 6.05e-07                           | 3.87e-07                           |
| 0.40        | 0.0824      | 1.1700                                | 0.0115    | 2.35  | 54.60             | 0.0242         | 0.0085           | 0.0032         | 3.40      | 1.62      | 0.2671                                  | 0.1793                                  | 5.89e-07                           | 3.87e-07                           |
| 0.50        | 0.0000      | 1.9100                                | 0.0115    | 2.20  | 103.00            | 0.0283         | 0.0099           | 0.0040         | 3.43      | 1.75      | 0.3985                                  | 0.2442                                  | 6.03e-07                           | 3.87e-07                           |
| 0.50        | 0.1092      | 1.3600                                | 0.0115    | 2.42  | 62.20             | 0.0213         | 0.0076           | 0.0027         | 3.42      | 1.58      | 0.3539                                  | 0.2527                                  | 5.83e-07                           | 3.87e-07                           |

$L_{ref} = 9.6$  in

Table 5. Relevant correlation parameters derived from the N-S database at the estimated unit  $Re_{\infty,inc}$  values for data obtained in the NASA LaRC 20-Inch  $CF_4$  Tunnel.

| $x/L_{ref}$ | $y/L_{ref}$ | $Re_{\infty}/ft$<br>( $1 \times 10^6$ ) | $k$ (in.) | $M_e$ | $Re_{\theta}/M_e$ | $\delta$ (in.) | $\delta^*$ (in.) | $\theta$ (in.) | $H_e/H_w$ | $T_e/T_w$ | $\rho_e u_e$<br>(lb-s/ft <sup>3</sup> ) | $\rho_k v_k$<br>(lb-s/ft <sup>3</sup> ) | $\mu_k$<br>(lb-s/ft <sup>2</sup> ) | $\mu_w$<br>(lb-s/ft <sup>2</sup> ) |
|-------------|-------------|---|-----------|-------|-------------------|----------------|------------------|----------------|-----------|-----------|---|---|------------------------------------|------------------------------------|
| 0.20        | 0.0000      | 0.4350                                  | 0.0065    | 2.05  | 78.20             | 0.0192         | 0.0056           | 0.0030         | 3.09      | 1.76      | 0.3682                                  | 0.2426                                  | 5.35e-07                           | 3.64e-07                           |
| 0.20        | 0.0177      | 0.4350                                  | 0.0065    | 2.07  | 74.40             | 0.0184         | 0.0053           | 0.0029         | 3.09      | 1.75      | 0.3717                                  | 0.2513                                  | 5.38e-07                           | 3.65e-07                           |
| 0.40        | 0.0000      | 0.2850                                  | 0.0065    | 2.41  | 73.70             | 0.0255         | 0.0079           | 0.0038         | 3.10      | 1.64      | 0.3060                                  | 0.1555                                  | 4.99e-07                           | 3.65e-07                           |
| 0.40        | 0.0706      | 0.4150                                  | 0.0065    | 2.46  | 74.80             | 0.0182         | 0.0055           | 0.0027         | 3.09      | 1.62      | 0.4465                                  | 0.2890                                  | 5.23e-07                           | 3.65e-07                           |
| 0.40        | 0.0605      | 0.2800                                  | 0.0065    | 2.49  | 63.80             | 0.0228         | 0.0069           | 0.0033         | 3.10      | 1.61      | 0.3087                                  | 0.1701                                  | 5.05e-07                           | 3.65e-07                           |
| 0.40        | 0.0000      | 0.2950                                  | 0.0115    | 2.40  | 75.10             | 0.0251         | 0.0077           | 0.0037         | 3.10      | 1.64      | 0.3168                                  | 0.2286                                  | 5.39e-07                           | 3.65e-07                           |
| 0.40        | 0.0605      | 0.2950                                  | 0.0115    | 2.48  | 65.60             | 0.0222         | 0.0068           | 0.0032         | 3.10      | 1.62      | 0.3236                                  | 0.2506                                  | 5.39e-07                           | 3.65e-07                           |
| 0.60        | 0.0000      | 0.3500                                  | 0.0065    | 2.54  | 97.00             | 0.0265         | 0.0083           | 0.0039         | 3.09      | 1.59      | 0.4059                                  | 0.2018                                  | 4.93e-07                           | 3.64e-07                           |
| 0.60        | 0.1370      | 0.3500                                  | 0.0065    | 2.70  | 55.60             | 0.0143         | 0.0042           | 0.0020         | 3.10      | 1.53      | 0.4781                                  | 0.3607                                  | 5.23e-07                           | 3.65e-07                           |
| 0.60        | 0.0000      | 0.2900                                  | 0.0115    | 2.57  | 87.50             | 0.0290         | 0.0091           | 0.0042         | 3.10      | 1.58      | 0.3403                                  | 0.2220                                  | 5.21e-07                           | 3.64e-07                           |
| 0.60        | 0.1429      | 0.2900                                  | 0.0115    | 2.77  | 42.80             | 0.0138         | 0.0041           | 0.0019         | 3.08      | 1.51      | 0.3840                                  | 0.3647                                  | 5.20e-07                           | 3.65e-07                           |
| 0.62        | 0.0000      | 0.1450                                  | 0.0115    | 2.67  | 61.40             | 0.0408         | 0.0129           | 0.0059         | 3.10      | 1.55      | 0.1761                                  | 0.0921                                  | 4.96e-07                           | 3.65e-07                           |
| 0.62        | 0.1489      | 0.2900                                  | 0.0115    | 2.78  | 40.70             | 0.0123         | 0.0038           | 0.0017         | 3.09      | 1.51      | 0.4089                                  | 0.4007                                  | 5.17e-07                           | 3.65e-07                           |
| 0.64        | 0.0000      | 0.3400                                  | 0.0065    | 2.57  | 98.40             | 0.0276         | 0.0087           | 0.0040         | 3.09      | 1.58      | 0.4007                                  | 0.1918                                  | 4.88e-07                           | 3.64e-07                           |
| 0.64        | 0.1701      | 0.3400                                  | 0.0065    | 2.83  | 25.80             | 0.0059         | 0.0016           | 0.0007         | 3.06      | 1.48      | 0.6003                                  | 0.6048                                  | 5.07e-07                           | 3.67e-07                           |
| 0.64        | 0.0000      | 0.2900                                  | 0.0115    | 2.60  | 90.20             | 0.0297         | 0.0094           | 0.0043         | 3.10      | 1.57      | 0.3440                                  | 0.2226                                  | 5.18e-07                           | 3.64e-07                           |
| 0.64        | 0.1701      | 0.1450                                  | 0.0115    | 2.86  | 16.40             | 0.0093         | 0.0024           | 0.0011         | 3.06      | 1.47      | 0.2511                                  | 0.2522                                  | 5.06e-07                           | 3.68e-07                           |
| 0.20        | 0.0000      | 0.3550                                  | 0.0115    | 2.55  | 59.60             | 0.0256         | 0.0082           | 0.0039         | 3.09      | 1.59      | 0.2539                                  | 0.1783                                  | 5.31e-07                           | 3.65e-07                           |
| 0.20        | 0.0370      | 0.3550                                  | 0.0115    | 2.66  | 50.40             | 0.0220         | 0.0069           | 0.0032         | 3.09      | 1.55      | 0.2656                                  | 0.2056                                  | 5.31e-07                           | 3.65e-07                           |
| 0.68        | 0.0000      | 0.4750                                  | 0.0065    | 2.55  | 122.00            | 0.0244         | 0.0077           | 0.0036         | 3.09      | 1.59      | 0.5566                                  | 0.2891                                  | 4.97e-07                           | 3.64e-07                           |
| 0.68        | 0.2111      | 0.2800                                  | 0.0065    | 2.81  | 17.20             | 0.0049         | 0.0012           | 0.0006         | 3.05      | 1.48      | 0.5260                                  | 0.5298                                  | 5.09e-07                           | 3.68e-07                           |
| 0.50        | 0.0000      | 0.2300                                  | 0.0115    | 3.07  | 61.80             | 0.0356         | 0.0128           | 0.0050         | 3.10      | 1.41      | 0.2226                                  | 0.1122                                  | 4.92e-07                           | 3.65e-07                           |
| 0.66        | 0.1937      | 0.2300                                  | 0.0065    | 3.20  | 15.10             | 0.0033         | 0.0009           | 0.0004         | 3.04      | 1.35      | 0.6891                                  | 0.6837                                  | 4.72e-07                           | 3.69e-07                           |
| 0.66        | 0.0000      | 0.3400                                  | 0.0115    | 3.13  | 87.30             | 0.0332         | 0.0121           | 0.0046         | 3.09      | 1.39      | 0.3392                                  | 0.1809                                  | 4.92e-07                           | 3.64e-07                           |
| 0.66        | 0.1937      | 0.1400                                  | 0.0115    | 3.20  | 11.80             | 0.0043         | 0.0012           | 0.0005         | 3.03      | 1.34      | 0.4149                                  | 0.4053                                  | 4.71e-07                           | 3.70e-07                           |

$L_{ref} = 9.6$  in

Table 6. Relevant correlation parameters derived from the N-S database at the estimated unit  $Re_{\infty,inc}$  values for data obtained at a nominal  $M = 10$  in the CUBRC LENS-I Shock Tunnel.

| $x/L_{ref}$ | $y/L_{ref}$ | $Re_{\infty}/ft$<br>( $1 \times 10^6$ ) | $k$ (in.) | $M_e$ | $Re_{\theta}/M_e$ | $\delta$ (in.) | $\delta^*$ (in.) | $\theta$ (in.) | $H_e/H_w$ | $T_e/T_w$ | $\rho_e v_e$<br>(lb-s/ft <sup>3</sup> ) | $\rho_k v_k$<br>(lb-s/ft <sup>3</sup> ) | $\mu_k$<br>(lb-s/ft <sup>2</sup> ) | $\mu_w$<br>(lb-s/ft <sup>2</sup> ) |
|-------------|-------------|---|-----------|-------|-------------------|----------------|------------------|----------------|-----------|-----------|---|---|------------------------------------|------------------------------------|
| 0.30        | 0.0000      | 0.4915                                  | 0.0192    | 1.63  | 71.10             | 0.0661         | 0.0161           | 0.0104         | 4.30      | 2.81      | 0.1030                                  | 0.0693                                  | 6.93e-07                           | 4.08e-07                           |
| 0.30        | -0.0454     | 0.6445                                  | 0.0191    | 1.68  | 71.60             | 0.0532         | 0.0130           | 0.0083         | 4.25      | 2.72      | 0.1317                                  | 0.0956                                  | 7.08e-07                           | 4.08e-07                           |
| 0.30        | 0.0454      | 0.6445                                  | 0.0198    | 1.68  | 71.60             | 0.0532         | 0.0130           | 0.0083         | 4.25      | 2.72      | 0.1317                                  | 0.0971                                  | 7.12e-07                           | 4.08e-07                           |

$L_{ref} = 23.04$  in

Table 7. Relevant correlation parameters derived from the N-S database at the estimated unit  $Re_{\infty,inc}$  values for data obtained at a nominal  $M = 16$  in the CUBRC LENS-I Shock Tunnel.

| $x/L_{ref}$ | $y/L_{ref}$ | $Re_{\infty}/ft$<br>( $1 \times 10^6$ ) | $k$ (in.) | $M_e$ | $Re_{\theta}/M_e$ | $\delta$ (in.) | $\delta^*$ (in.) | $\theta$ (in.) | $H_e/H_w$ | $T_e/T_w$ | $\rho_e v_e$<br>(lb-s/ft <sup>3</sup> ) | $\rho_k v_k$<br>(lb-s/ft <sup>3</sup> ) | $\mu_k$<br>(lb-s/ft <sup>2</sup> ) | $\mu_w$<br>(lb-s/ft <sup>2</sup> ) |
|-------------|-------------|---|-----------|-------|-------------------|----------------|------------------|----------------|-----------|-----------|---|---|------------------------------------|------------------------------------|
| 0.50        | 0.0000      | 0.7105                                  | 0.0201    | 1.88  | 79.60             | 0.0775         | 0.0160           | 0.0129         | 9.24      | 5.43      | 0.1657                                  | 0.1165                                  | 1.03e-06                           | 4.08e-07                           |
| 0.50        | -0.1008     | 1.3300                                  | 0.0189    | 1.90  | 88.70             | 0.0449         | 0.0094           | 0.0073         | 8.97      | 5.22      | 0.3210                                  | 0.2601                                  | 1.12e-06                           | 4.08e-07                           |
| 0.50        | 0.1008      | 1.1060                                  | 0.0188    | 1.92  | 80.40             | 0.0490         | 0.0103           | 0.0080         | 9.05      | 5.22      | 0.2698                                  | 0.2108                                  | 1.10e-06                           | 4.08e-07                           |
| 0.50        | 0.0000      | 0.2130                                  | 0.1816    | 2.01  | 43.60             | 0.1340         | 0.0293           | 0.0216         | 8.90      | 4.94      | 0.0545                                  | 0.0573                                  | 1.10e-06                           | 4.08e-07                           |
| 0.74        | 0.0000      | 0.4290                                  | 0.0222    | 2.06  | 78.10             | 0.1140         | 0.0250           | 0.0182         | 9.59      | 5.19      | 0.1228                                  | 0.0765                                  | 9.52e-07                           | 4.08e-07                           |
| 0.74        | -0.2350     | 0.4290                                  | 0.0176    | 2.17  | 34.20             | 0.0410         | 0.0068           | 0.0062         | 9.57      | 4.94      | 0.1615                                  | 0.1414                                  | 1.06e-06                           | 4.08e-07                           |
| 0.50        | 0.0970      | 0.4290                                  | 0.0229    | 2.01  | 51.50             | 0.0781         | 0.0164           | 0.0125         | 9.57      | 5.31      | 0.1172                                  | 0.0838                                  | 1.07e-06                           | 4.08e-07                           |
| 0.10        | 0.0000      | 0.4620                                  | 0.2096    | 1.31  | 38.30             | 0.0599         | 0.0081           | 0.0108         | 9.55      | 7.11      | 0.0795                                  | 0.1068                                  | 1.32e-06                           | 4.08e-07                           |
| 0.30        | -0.0454     | 0.2575                                  | 0.2075    | 1.89  | 35.10             | 0.0992         | 0.0200           | 0.0163         | 9.12      | 5.33      | 0.0576                                  | 0.0650                                  | 1.12e-06                           | 4.08e-07                           |
| 0.30        | 0.0454      | 0.2575                                  | 0.2077    | 1.89  | 35.10             | 0.0992         | 0.0200           | 0.0163         | 9.12      | 5.33      | 0.0576                                  | 0.0650                                  | 1.12e-06                           | 4.08e-07                           |
| *0.50       | -0.1008     | 0.2760                                  | 0.1685    | 2.07  | 40.39             | 0.0941         | 0.0206           | 0.0148         | 9.20      | 4.95      | 0.0763                                  | 0.0843                                  | 1.07e-06                           | 4.08e-07                           |
| *0.50       | 0.1008      | 0.2760                                  | 0.1688    | 2.07  | 40.39             | 0.0941         | 0.0206           | 0.0148         | 9.20      | 4.95      | 0.0763                                  | 0.0843                                  | 1.07e-06                           | 4.08e-07                           |

$L_{ref} = 23.04$  in

\* The flow remained laminar downstream of these attachment-line trips for this test configuration (i.e., test configuration 4 as noted in Ref. [24]). The correlation parameters at the highest unit  $Re_{\infty}$  tested are shown above in the last two lines of the table for completeness.

Table 8. Historical flight cases as documented in Refs. [5] and [26].

| <b>Flight</b> | <b>Gap Filler</b> | <b>X – 236 (in.)</b> | <b>Y (in.)</b> | <b>Z (in.)</b> | <b>k (in.)</b>                   | <b>Transition time (s)</b> |
|---------------|-------------------|----------------------|----------------|----------------|----------------------------------|----------------------------|
| STS-28        | A-28              | 329.00               | -21.00         | 278.00         | $0.5 \pm 0.1$ ( $\pm 20\%$ )     | 902                        |
| STS-28        | B-28              | 528.00               | -94.00         | 282.00         | $0.5 \pm 0.1$ ( $\pm 20\%$ )     | 912                        |
| STS-41        | C-41              | 274.90               | -45.60         | 281.60         | $0.11 \pm 0.01$ ( $\pm 9\%$ )    | 1201                       |
| STS-55        | A-55              | 225.10               | -2.10          | 278.00         | $0.20 \pm 0.05$ ( $\pm 25\%$ )   | 1060                       |
| STS-55        | C-55              | 181.60               | -20.20         | 282.90         | $0.20 \pm 0.05$ ( $\pm 25\%$ )   | 1060                       |
| STS-73        | A-73              | 279.18               | 7.43           | 278.61         | $0.60 \pm 0.11$ ( $\pm 18\%$ )   | 880                        |
| *STS-73       | A-73              | 279.18               | 7.43           | 278.61         | $0.60 \pm 0.11$ ( $\pm 18\%$ )   | 982                        |
| *STS-73       | A-73              | 279.18               | 7.43           | 278.61         | $1.40 \pm 0.19$ ( $\pm 14\%$ )   | 880                        |
| STS-81        | A-81              | 235.16               | 9.02           | 279.79         | $0.32 \pm 0.03$ ( $\pm 9\%$ )    | 966                        |
| STS-94        | A-94              | 211.20               | 4.24           | 280.74         | $0.30 \pm 0.08$ ( $\pm 27\%$ )   | 993                        |
| STS-99        | A-99              | 267.50               | -6.40          | 278.80         | $0.35 \pm 0.09$ ( $\pm 26\%$ )   | 1012                       |
| STS-103       | A-103             | 270.70               | 7.43           | 278.78         | $0.250 \pm 0.075$ ( $\pm 30\%$ ) | 958                        |

\* Alternate interpretation of data.

Table 9. Relevant correlation parameters for historical flight cases.

| STS | $x/L_{ref}$ | $y/L_{ref}$ | $Re_{\infty}/ft$<br>( $1 \times 10^6$ ) | $k$ (in.) | $M_e$ | $Re_{\theta}/M_e$ | $\delta$ (in.) | $\delta^*$ (in.) | $\theta$ (in.) | $H_e/H_w$ | $T_e/T_w$ | $\rho_e u_e$<br>(lb-s/ft <sup>3</sup> ) | $\rho_k v_k$<br>(lb-s/ft <sup>3</sup> ) | $\mu_k$<br>(lb-s/ft <sup>2</sup> ) | $\mu_w$<br>(lb-s/ft <sup>2</sup> ) |
|-----|-------------|-------------|---|-----------|-------|-------------------|----------------|------------------|----------------|-----------|-----------|---|---|------------------------------------|------------------------------------|
| 28  | 0.2570      | -0.0164     | 0.0227                                  | 0.5000    | 2.02  | 154.79            | 1.7870         | 0.4166           | 0.2942         | 3.68      | 4.27      | 0.0331                                  | 0.0222                                  | 2.30e-06                           | 8.65e-07                           |
| 28  | 0.4125      | -0.0734     | 0.0246                                  | 0.5000    | 2.38  | 144.59            | 1.4804         | 0.3624           | 0.2317         | 3.89      | 3.87      | 0.0429                                  | 0.0331                                  | 2.18e-06                           | 8.83e-07                           |
| 41  | 0.2148      | -0.0356     | 0.0731                                  | 0.1100    | 1.62  | 256.42            | 0.8692         | 0.1689           | 0.1257         | 4.01      | 2.57      | 0.0522                                  | 0.0327                                  | 1.07e-06                           | 7.19e-07                           |
| 55  | 0.1758      | -0.0017     | 0.0463                                  | 0.2000    | 1.68  | 241.39            | 1.1131         | 0.2218           | 0.1839         | 3.26      | 3.43      | 0.0540                                  | 0.0370                                  | 1.66e-06                           | 8.42e-07                           |
| 55  | 0.1419      | -0.0157     | 0.0463                                  | 0.2000    | 1.58  | 215.32            | 0.9535         | 0.1841           | 0.1579         | 3.18      | 3.36      | 0.0538                                  | 0.0353                                  | 1.50e-06                           | 8.67e-07                           |
| 73  | 0.2181      | 0.0058      | 0.0194                                  | 0.6000    | 2.12  | 135.25            | 1.8958         | 0.4316           | 0.3199         | 3.83      | 4.32      | 0.0291                                  | 0.0204                                  | 2.40e-06                           | 8.79e-07                           |
| *73 | 0.2181      | 0.0058      | 0.0276                                  | 0.6000    | 1.80  | 175.10            | 1.5660         | 0.3469           | 0.2662         | 3.53      | 4.12      | 0.0364                                  | 0.0289                                  | 2.35e-06                           | 8.83e-07                           |
| *73 | 0.2181      | 0.0058      | 0.0194                                  | 1.4000    | 2.12  | 135.25            | 1.8958         | 0.4316           | 0.3199         | 3.83      | 4.32      | 0.0291                                  | 0.0254                                  | 2.75e-06                           | 8.79e-07                           |
| 81  | 0.1837      | 0.0070      | 0.0323                                  | 0.3200    | 1.84  | 182.45            | 1.4761         | 0.3124           | 0.2435         | 3.71      | 4.01      | 0.0409                                  | 0.0268                                  | 2.03e-06                           | 8.81e-07                           |
| 94  | 0.1651      | 0.0033      | 0.0371                                  | 0.3000    | 1.74  | 194.11            | 1.3220         | 0.2675           | 0.2213         | 3.66      | 3.90      | 0.0443                                  | 0.0302                                  | 1.95e-06                           | 8.85e-07                           |
| 99  | 0.2090      | -0.0049     | 0.0310                                  | 0.3500    | 1.82  | 191.88            | 1.5383         | 0.3307           | 0.2545         | 3.76      | 4.08      | 0.0410                                  | 0.0268                                  | 2.08e-06                           | 8.77e-07                           |
| 103 | 0.2115      | 0.0058      | 0.0338                                  | 0.2500    | 1.81  | 197.39            | 1.3929         | 0.2950           | 0.2326         | 3.47      | 3.91      | 0.0429                                  | 0.0313                                  | 2.06e-06                           | 8.56e-07                           |

$L_{ref} = 1280$  in

\* Alternate interpretation of data (same sequential order as Table 8).

Table 10. Side-by-side comparison of facility dependent metrics for a correlation in the form of the approved BLT Tool V.1 protuberance correlation,  $Re_{\theta}/M_e = C \times (k/\delta)^n$ , using both LATCH and N-S databases with  $n = -1$ .

| Facility                             | N   | LATCH Database |    |             |             |              |       |              | Navier-Stokes Database |    |             |             |              |       |              |
|--------------------------------------|-----|----------------|----|-------------|-------------|--------------|-------|--------------|------------------------|----|-------------|-------------|--------------|-------|--------------|
|                                      |     | C              | n  | $C_{+95\%}$ | $C_{-95\%}$ | $\Delta C/C$ | R     | $\sigma_C/C$ | C                      | n  | $C_{+95\%}$ | $C_{-95\%}$ | $\Delta C/C$ | R     | $\sigma_C/C$ |
| LaRC M6: Existing Data               | 44  | 37.3           | -1 | 59.5        | 23.4        | 0.97         | -0.77 | -            | 35.5                   | -1 | 56.7        | 22.3        | 0.97         | -0.93 | -            |
| LaRC M6: New Data                    | 22  | 39.9           | -1 | 81.6        | 19.5        | 1.56         | -0.44 | -            | 39.2                   | -1 | 75.4        | 20.4        | 1.40         | -0.71 | -            |
| LaRC M10: Existing Data              | 24  | 26.4           | -1 | 38.0        | 18.3        | 0.75         | -0.81 | -            | 30.0                   | -1 | 41.4        | 21.8        | 0.65         | -0.92 | -            |
| LaRC CF <sub>4</sub> : Existing Data | 25  | 22.8           | -1 | 38.0        | 13.7        | 1.07         | -0.86 | -            | 26.8                   | -1 | 42.7        | 16.8        | 0.97         | -0.94 | -            |
| LENS M10: New Data                   | 3   | 20.1           | -1 | 33.6        | 12.0        | 1.08         | 0.99  | -            | 24.2                   | -1 | 35.7        | 16.4        | 0.80         | 0.99  | -            |
| LENS M16: New Data                   | 10  | 32.9           | -1 | 162.5       | 6.7         | 4.73         | -0.75 | n/a          | 35.8                   | -1 | 191.4       | 6.7         | 5.16         | -0.73 | n/a          |
| <b>Ensemble</b>                      | 124 | 30.6           | -1 | 62.6        | 14.9        | 1.56         | -0.62 | 30.2%        | 31.9                   | -1 | 57.8        | 17.6        | 1.26         | -0.87 | 19.9%        |

\* Note that the LENS M16 data are not used in the computation of  $\sigma_C/\bar{C}$ .

Table 11. Down-select table for most promising correlations investigated.

| Proposed Equation | Correlation Equation<br>$C =$                             | Ground-Based |              |              | Ground-Based + Flight |              |              |
|-------------------|---|--------------|--------------|--------------|-----------------------|--------------|--------------|
|                   |   | $R$          | $\Delta C/C$ | $\sigma_C/C$ | $R$                   | $\Delta C/C$ | $\sigma_C/C$ |
| 1                 | $Re_\theta/M_e \cdot k/\delta$                            | -0.87        | 1.26         | 19.9%        | -0.88                 | 1.25         | 21.2%        |
| 2                 | $Re_\theta/M_e \cdot k/\delta^*$                          | -0.90        | 1.08         | 7.3%         | -0.87                 | 1.32         | 34.9%        |
| 3                 | $Re_\theta/M_e \cdot k/\theta$                            | -0.84        | 1.41         | 25.9%        | -0.86                 | 1.36         | 23.3%        |
| 4                 | $Re_\theta/M_e \cdot (k/\delta)(T_e/T_w)^{0.16}$          | -0.89        | 1.14         | 14.5%        | -0.89                 | 1.20         | 23.6%        |
| ⇒ 5               | $Re_\theta/M_e \cdot (k/\delta)(H_e/H_w)^{0.30}$          | -0.91        | 1.04         | 8.9%         | -0.91                 | 1.10         | 19.9%        |
| 6                 | $\rho_k u_k k/\mu_w$                                      | -0.79        | 2.51         | 30.9%        | –                     | –            | –            |
| ⇒ 7               | $*Re_k^{0.6} \cdot [Re_\theta \cdot (\mu_e/\mu_k)]^{0.4}$ | -0.87        | 1.09         | 14.8%        | -0.84                 | 1.30         | 35.0%        |

\* Results are for  $n = -0.6$  for all data (see Eq. 14).

⇒ Recommended correlations.

Table 12. Tabulated correlation coefficients for proposed correlations 5 and 7 based on the approach adopted by the Aeroheating Panel and the use of the entire ensemble (ground-based and flight) database.

| Approach                               | Correlation | $C_{-95\%}$ | $C$ (Best Fit) | $C_{+95\%}$ |
|--|-------------|-------------|----------------|-------------|
| BF(flight) + $2\sigma$ (ground-based)* | PC#5        | 35.3        | 61.3           | 106.4       |
| Ensemble(ground-based & flight)        | PC#5        | 25.3        | 42.8           | 72.5        |
| BF(flight) + $2\sigma$ (ground-based)* | PC#7        | 220.7       | 396.8          | 713.4       |
| Ensemble(ground-based & flight)        | PC#7        | 118.0       | 217.6          | 401.3       |

\* Approach adopted by Aeroheating Panel (BLT Tool V.2).

Table 13. Computed transition times for the ten accepted flight cases using proposed correlations 5 and 7 with the correlation coefficients recommended by the Aeroheating Panel. The three predicted transition times are the 95% bounding times and best estimate (BE) time, all with the quoted protuberance heights  $k$ .

| Flight   | Gap Filler   | $X - 236$ (in.) | $Y$ (in.) | $Z$ (in.) | $k$ (in.) | Transition time (s) | Predicted Transition Times (s) |      |        |        |      |        |
|----------|--------------|-----------------|-----------|-----------|-----------|---------------------|--------------------------------|------|--------|--------|------|--------|
|          |              |                 |           |           |           |                     | (-95%)                         | (BE) | (+95%) | (-95%) | (BE) | (+95%) |
| STS-28   | A-28         | 329.00          | -21.00    | 278.00    | 0.50      | 902                 | 773                            | 892  | 982    | 738    | 914  | 1065   |
| STS-28   | B-28         | 528.00          | -94.00    | 282.00    | 0.50      | 912                 | 766                            | 888  | 974    | 720    | 892  | 997    |
| STS-41   | C-41         | 274.90          | -45.60    | 281.60    | 0.11      | 1201                | 1109                           | 1254 | >1262  | 969    | 1229 | >1262  |
| STS-55   | A-55         | 225.10          | -2.10     | 278.00    | 0.20      | 1060                | 969                            | 1064 | 1252   | 926    | 1056 | 1285   |
| STS-55   | C-55         | 181.60          | -20.20    | 282.90    | 0.20      | 1060                | 961                            | 1057 | 1243   | 941    | 1073 | 1295   |
| STS-73   | A-73         | 279.18          | 7.43      | 278.61    | 0.60      | 880                 | 752                            | 889  | 999    | 718    | 911  | 1062   |
| STS-81   | A-81         | 235.16          | 9.02      | 279.79    | 0.32      | 966                 | 878                            | 971  | 1115   | 839    | 981  | 1249   |
| STS-94   | A-94         | 211.20          | 4.24      | 280.74    | 0.30      | 993                 | 885                            | 981  | 1106   | 855    | 1000 | 1253   |
| STS-99   | A-99         | 267.50          | -6.40     | 278.80    | 0.35      | 1012                | 902                            | 1004 | 1115   | 847    | 1015 | 1247   |
| STS-103  | A-103        | 270.70          | 7.43      | 278.78    | 0.25      | 958                 | 897                            | 984  | 1191   | 857    | 973  | 1227   |
| *STS-121 | RPM-700.3-01 | 1261.69         | -351.64   | 293.46    | 0.40      | 938                 | 747                            | 877  | 994    | 685    | 838  | 969    |

\* Post STS-107 Shuttle mission (not part of calibrated flight data used for tool development) where  $k$  was measured post landing.

Table 14. Revisited correlations and the respective metrics.

| Correlation Equation   | Ground-Based + Flight |              |              |
|--|-----------------------|--------------|--------------|
|  | $R$                   | $\Delta C/C$ | $\sigma_C/C$ |
| $*Re_\theta/M_e \cdot (k/\delta)(H_e/H_w)^{0.30} = C$            | -0.91                 | 1.10         | 19.9%        |
| $Re_\theta/M_e \cdot (k/\delta^*)(T_e/T_w)^{-0.27} = C$          | -0.89                 | 1.20         | 23.5%        |
| $Re_\theta/M_e \cdot (k/\delta^*)(H_e/H_w)^{-0.10} = C$          | -0.87                 | 1.31         | 33.2%        |
| $Re_\theta/M_e \cdot (k/\theta)(T_e/T_w)^{0.33} = C$             | -0.89                 | 1.17         | 23.5%        |
| $\Rightarrow Re_\theta/M_e \cdot (k/\theta)(H_e/H_w)^{0.44} = C$ | -0.92                 | 1.05         | 15.5%        |

\* Proposed correlation #5 used as baseline reference.

$\Rightarrow$  Improved correlations.



Figure 1. Focused inspection image of a protruding gap filler on STS-121.

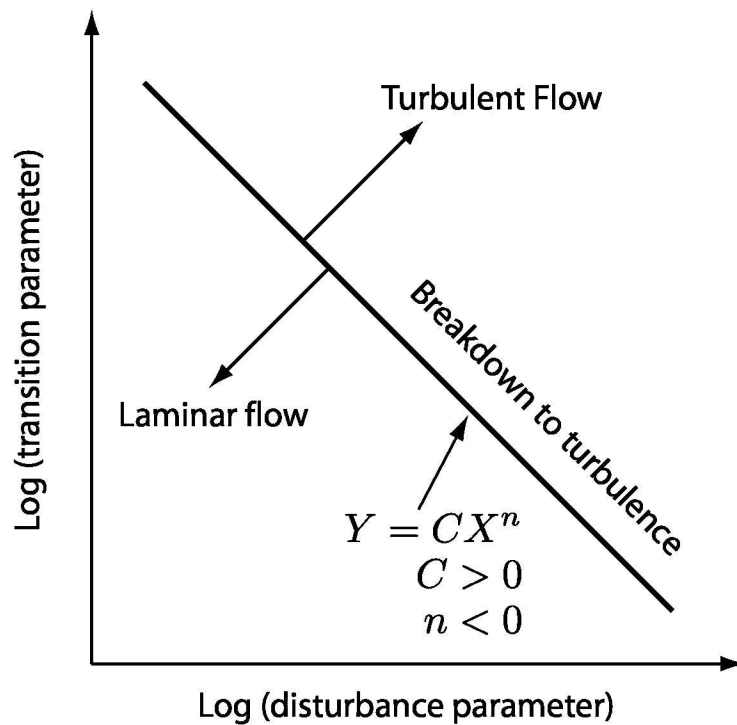


Figure 2. Generalized correlation approach used in this report.

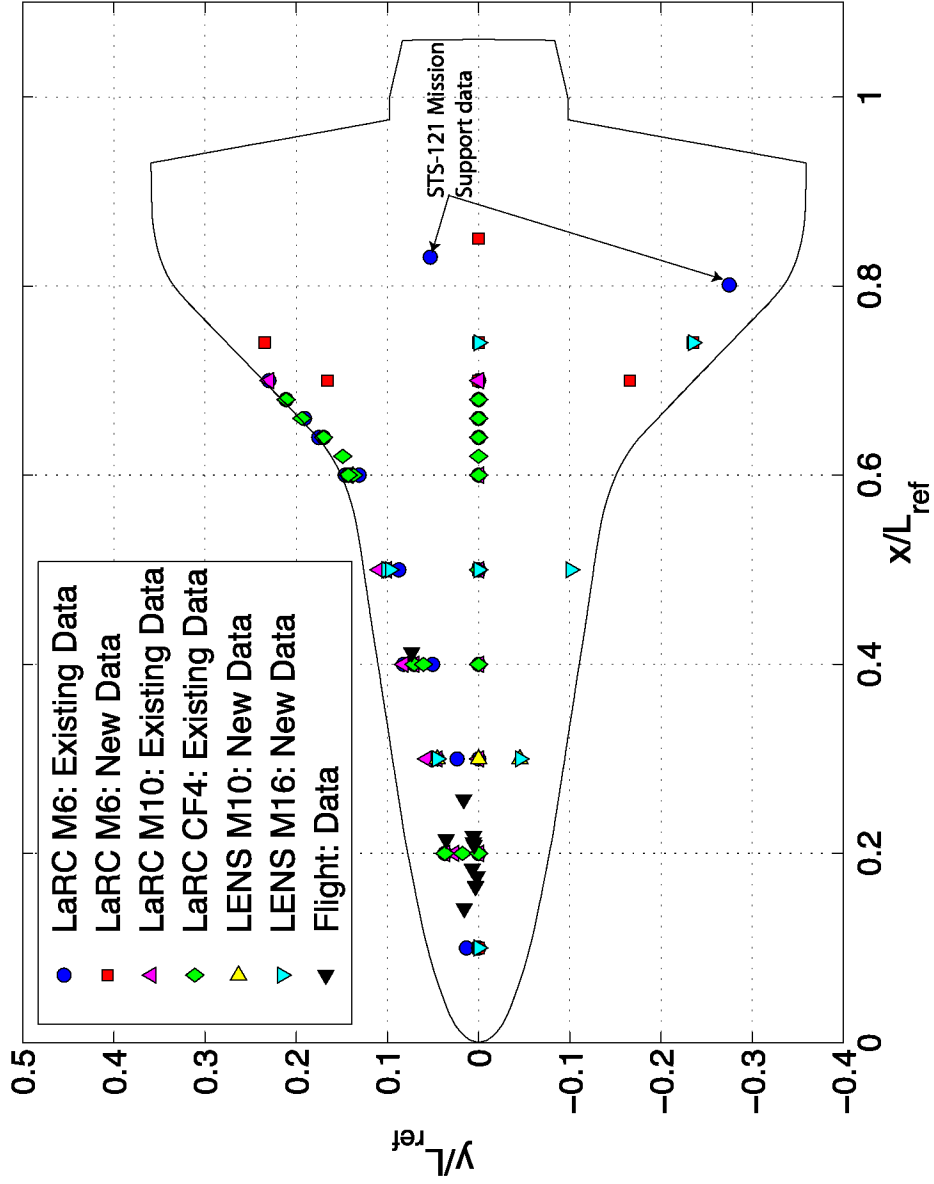


Figure 3. Complete database (ground-based and flight) projected onto windward surface. Note that the STS-121 mission support data are highlighted. The remaining M6 existing data, obtained the 20-Inch Mach 6 Air Tunnel, were acquired prior to the BLT Tool V.1 development. Viewed from top of Orbiter.

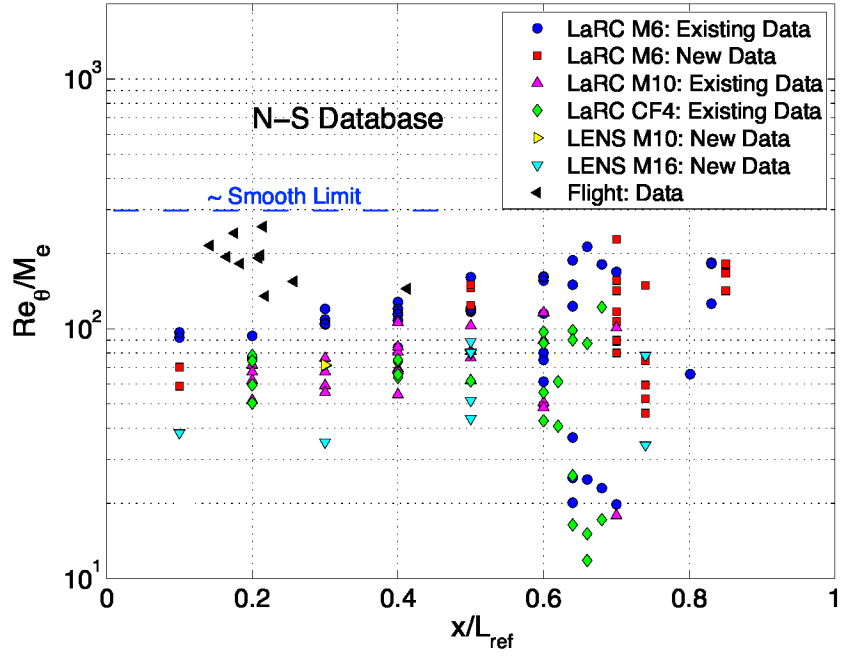


Figure 4. Complete database (ground-based and flight) in the form of  $Re_\theta/M_e$  versus  $x/L_{ref}$ .

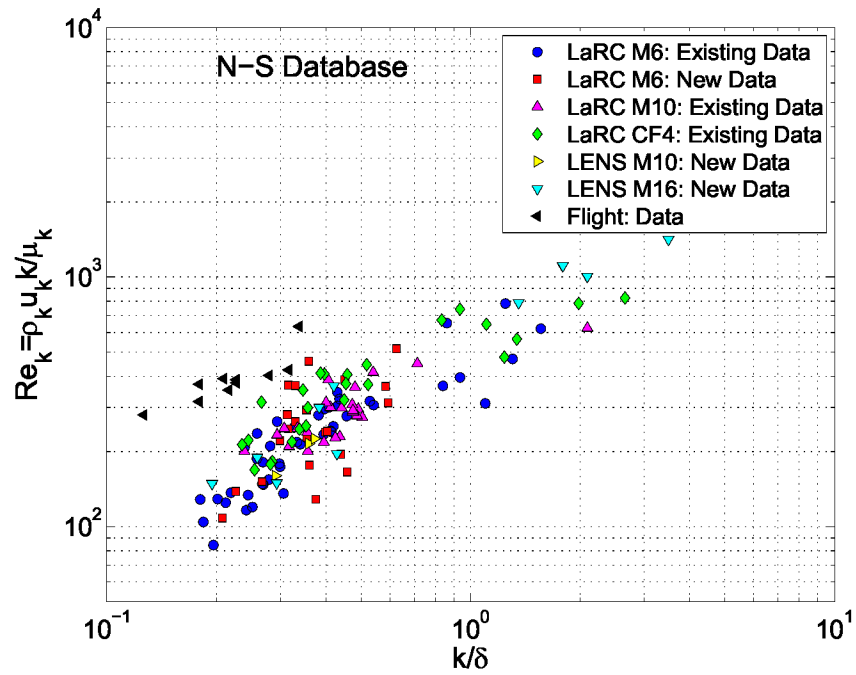


Figure 5. Complete database (ground-based and flight) in the form of  $Re_k$  versus  $k/\delta$ .

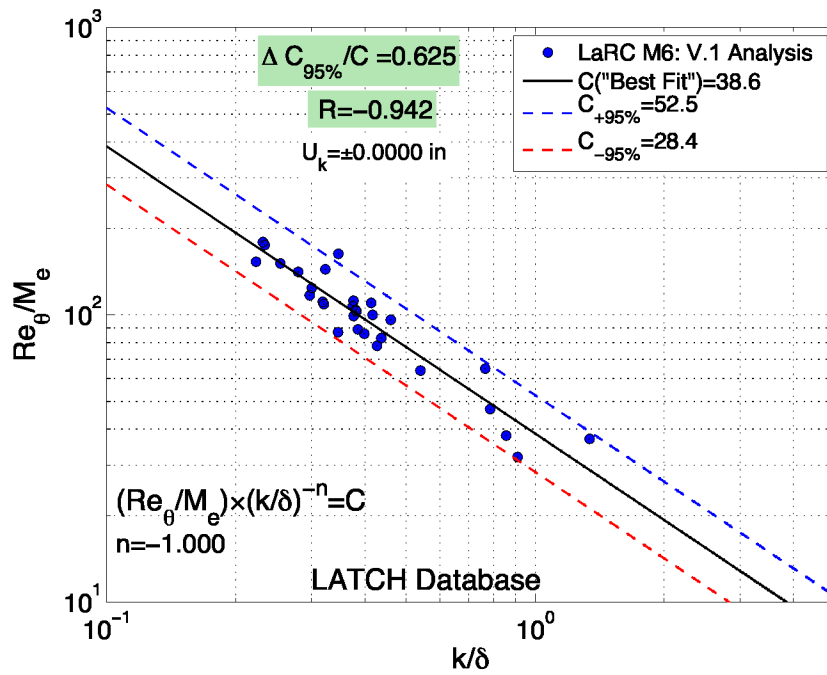


Figure 6. Existing LaRC 20-Inch Mach 6 Air Tunnel data used to develop BLT Tool V.1.

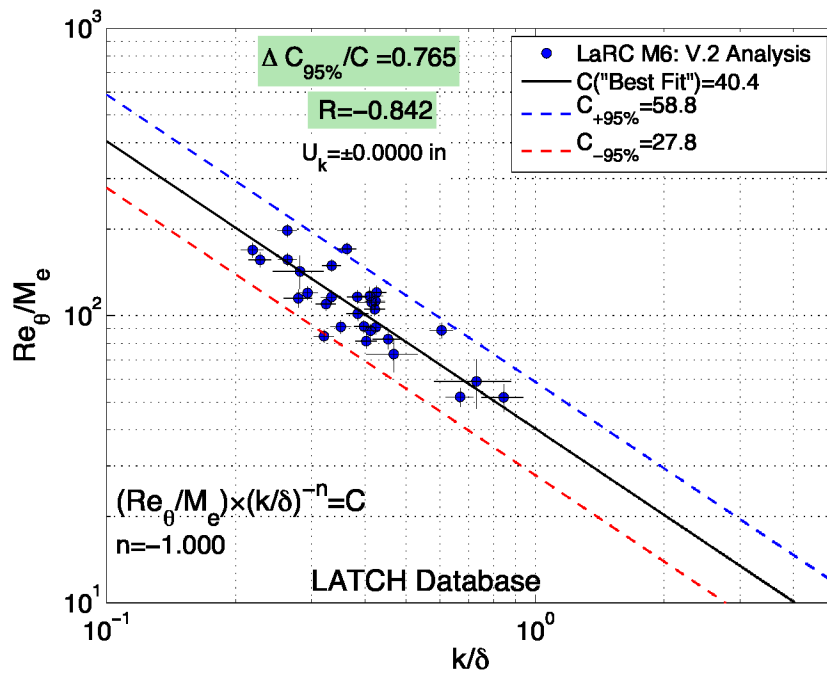


Figure 7. Existing LaRC 20-Inch Mach 6 Air Tunnel data reanalyzed to estimate the incipient transition Reynolds number as the average of the last laminar value and the first value with laminar departure.

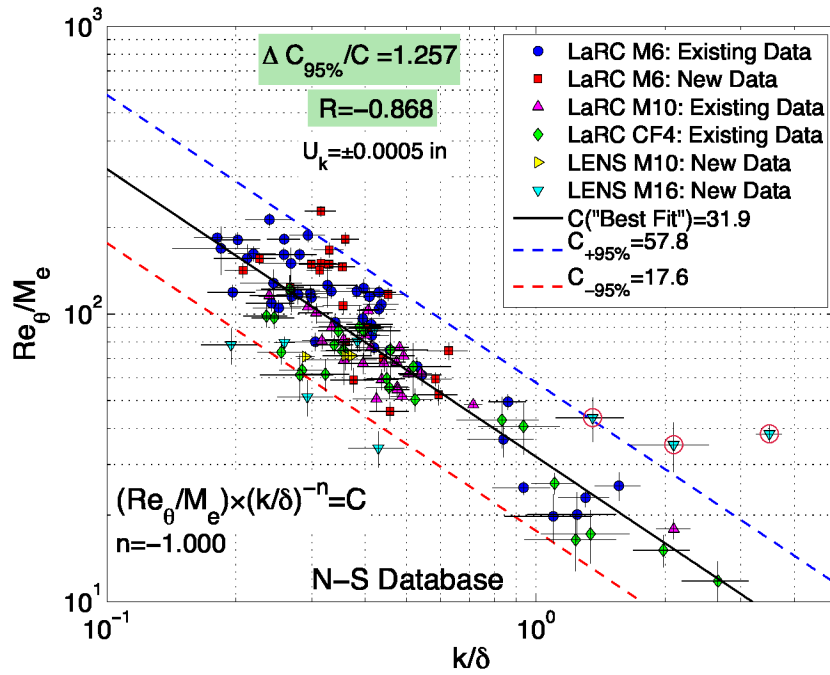


Figure 8. Ensemble of facility dependent data based on N-S database.

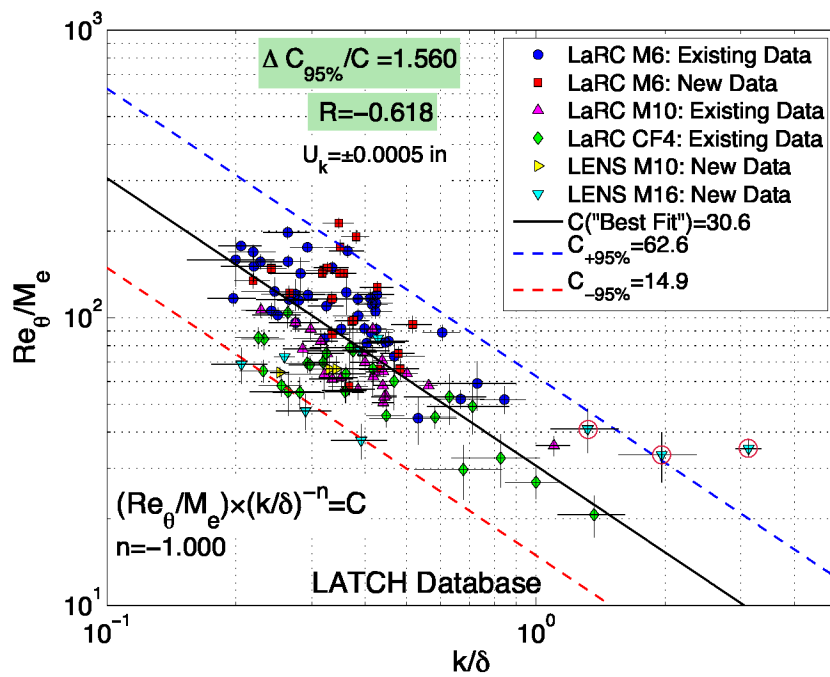


Figure 9. Ensemble of facility dependent data based on LATCH database.

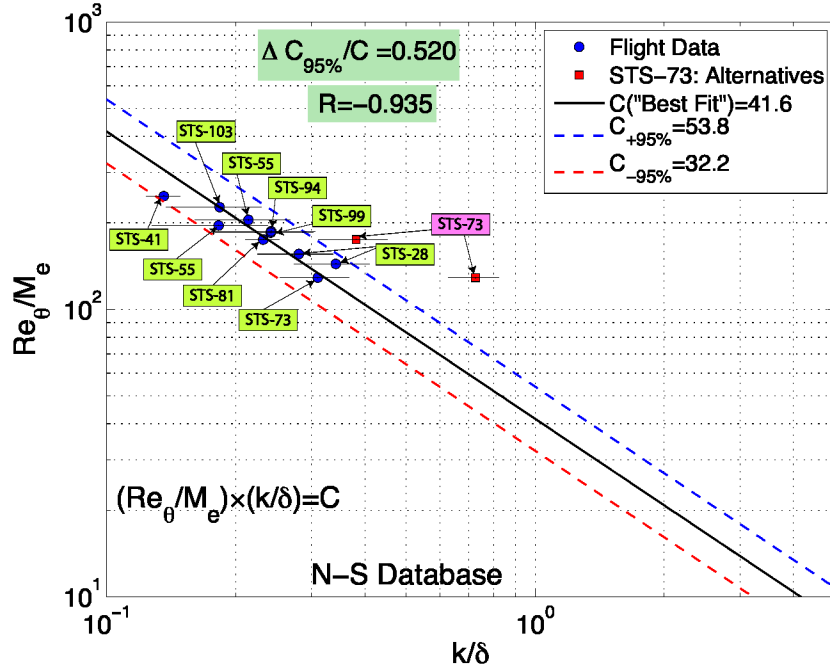


Figure 10. Calibrated flight data analyzed using N-S database.

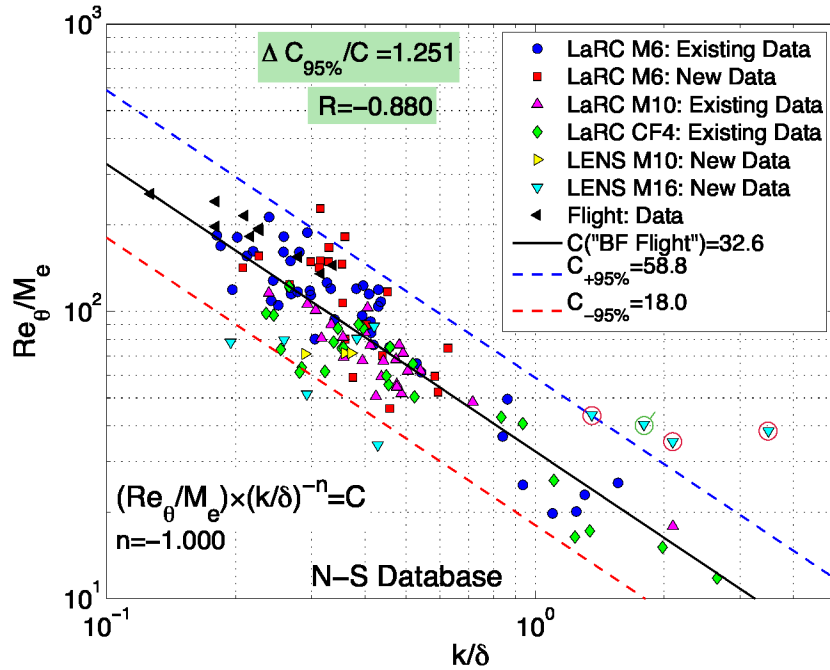


Figure 11. Ensemble of facility dependent data and flight data based on N-S database for correlation  $Re_{\theta}/M_e \times k/\delta = C$ .

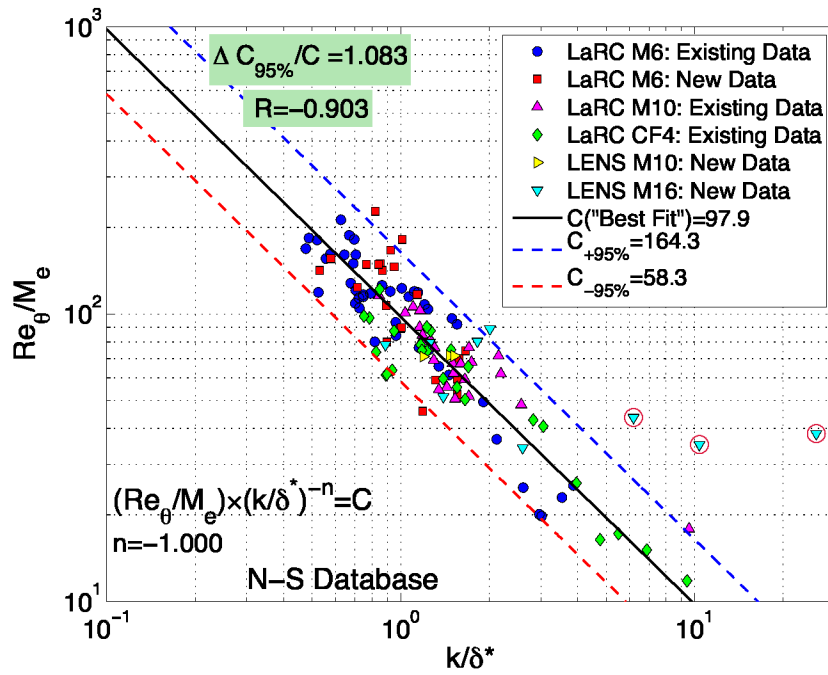


Figure 12. Ensemble of facility dependent data based on N-S database for correlation  $Re_{\theta}/M_e \times k/\delta^* = C$ .

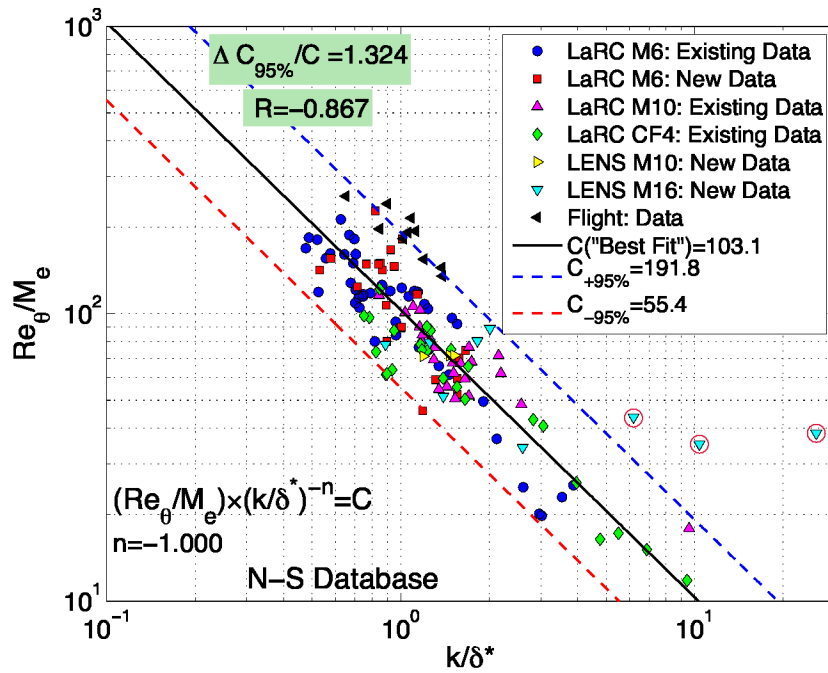


Figure 13. Ensemble of facility dependent data and flight data based on N-S database for correlation  $Re_{\theta}/M_e \times k/\delta^* = C$ .

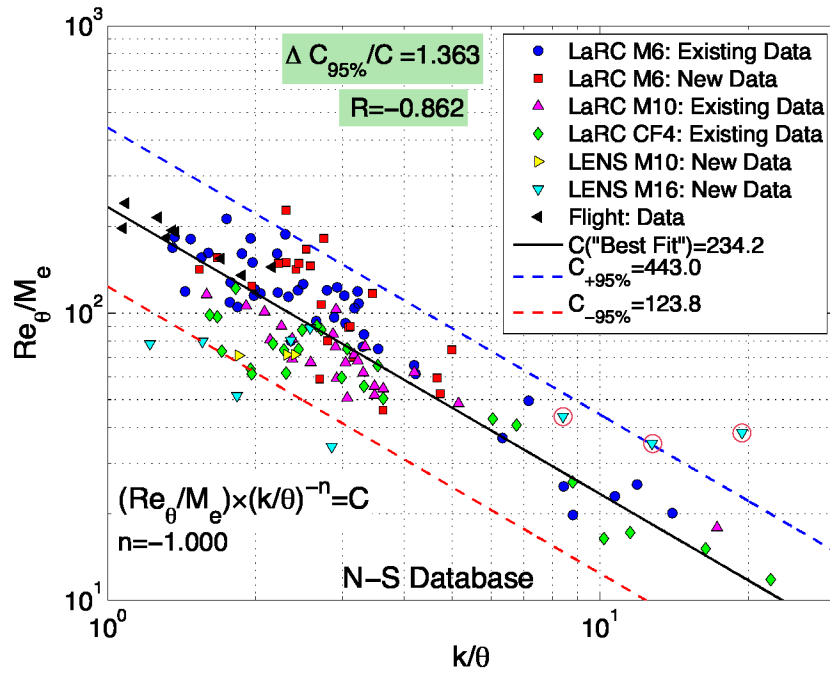


Figure 14. Ensemble of facility dependent data and flight data based on N-S database for correlation  $Re_{\theta}/M_e \times k/\theta = C$ .

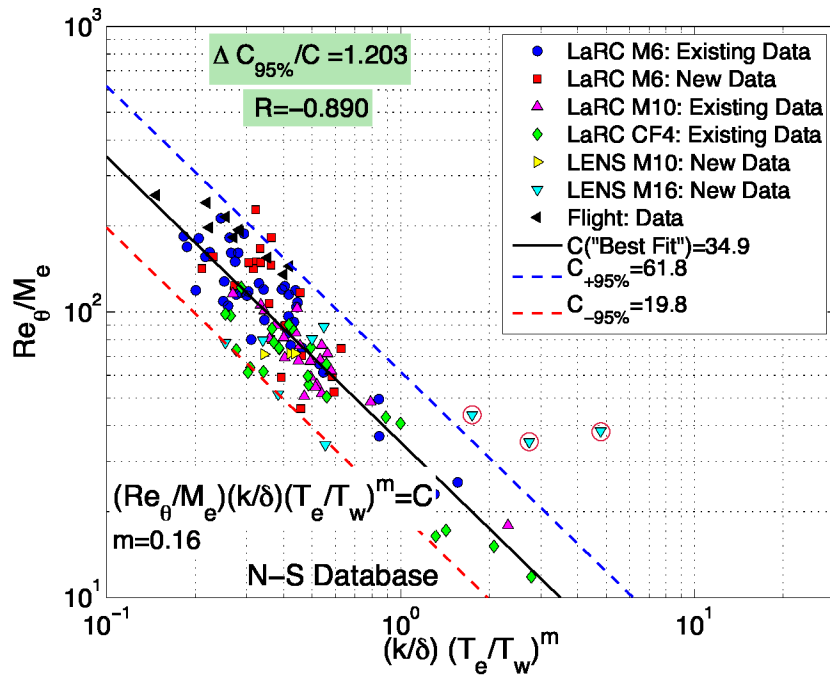


Figure 15. Ensemble of facility dependent data and flight data based on N-S database for correlation  $Re_{\theta}/M_e \times (k/\delta)(T_e/T_w)^{0.16} = C$ .

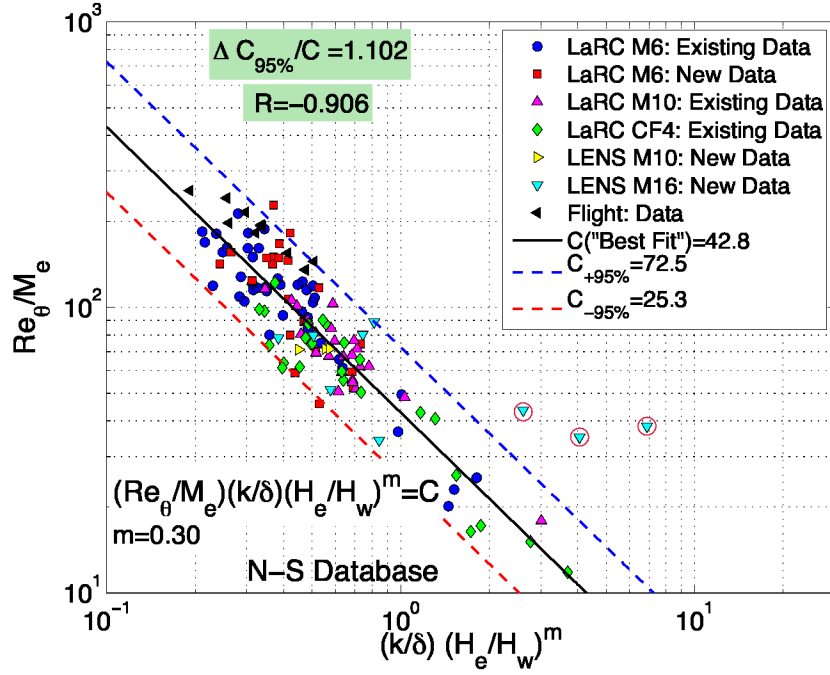


Figure 16. Ensemble of facility dependent data and flight data based on N-S database for correlation  $Re_\theta/M_e \times (k/\delta)(H_e/H_w)^{0.30} = C$ .

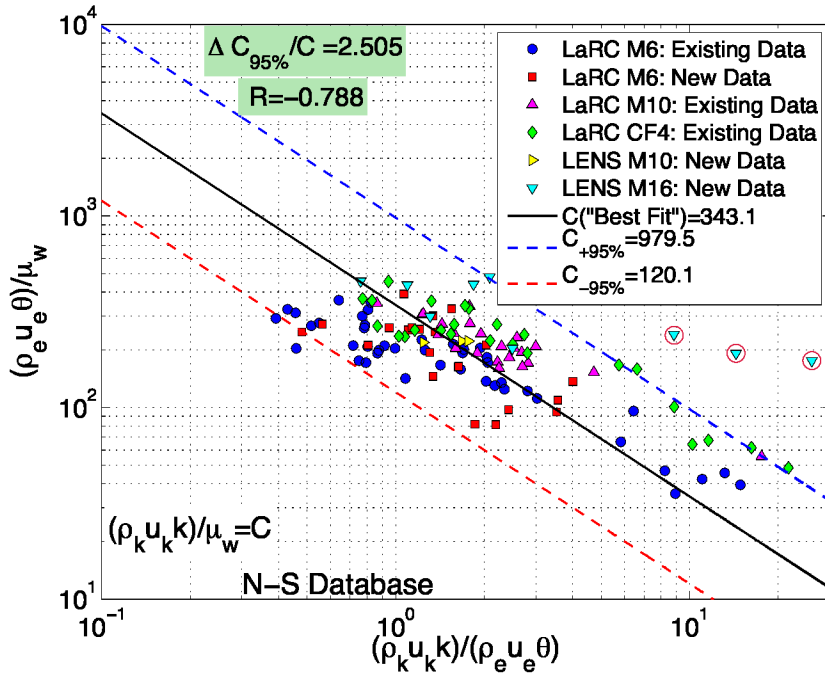


Figure 17. Ensemble of facility dependent data based on N-S database for correlation  $Re_k$  (reference to  $\mu_w$ ) =  $C$ .

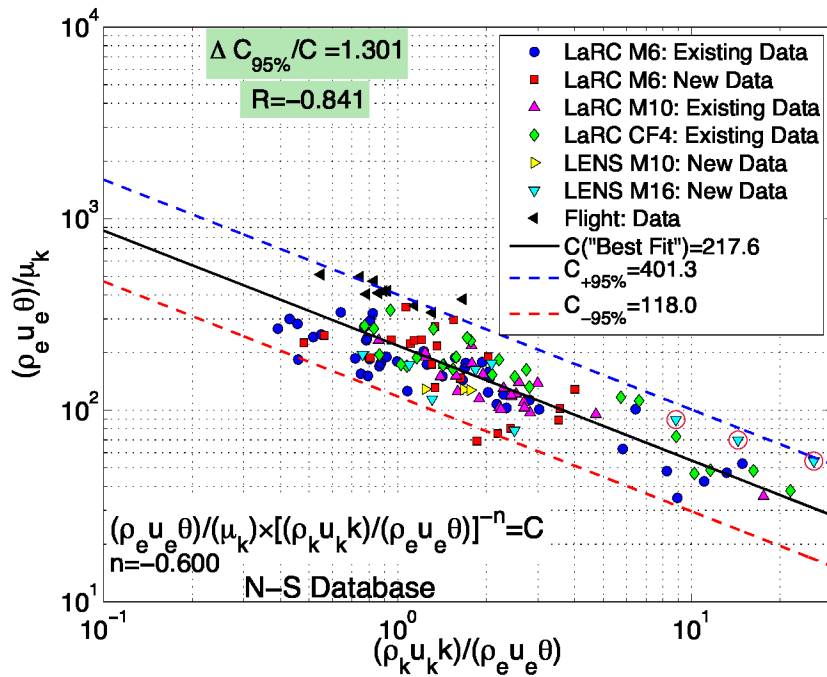


Figure 18. Ensemble of facility dependent data and flight data based on N-S database for correlation of the  $Re_k$ -type.

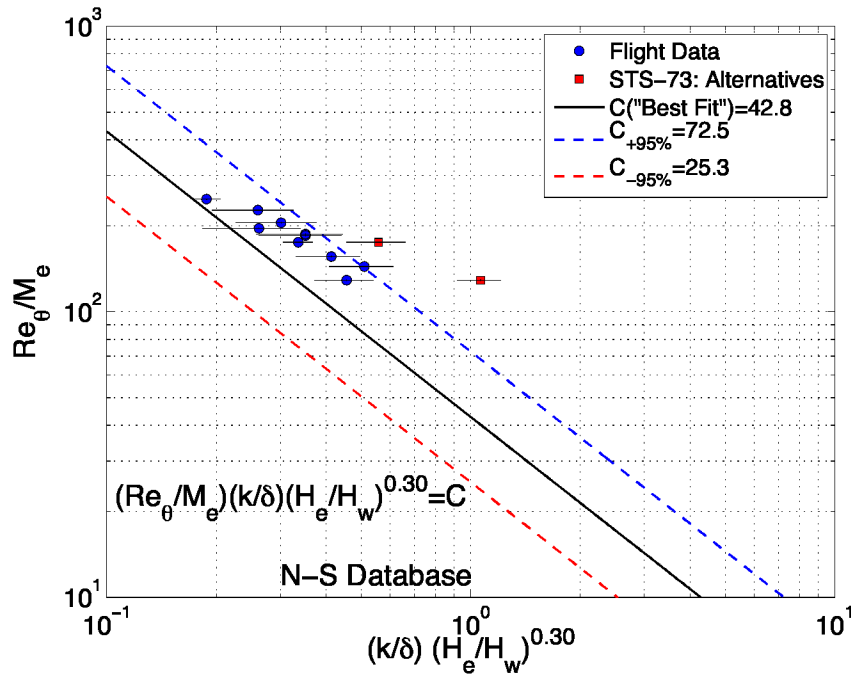


Figure 19. Flight data plotted in correlation space (PC#5) along with correlation curves derived from ensemble of facility dependent and flight data (N-S database).

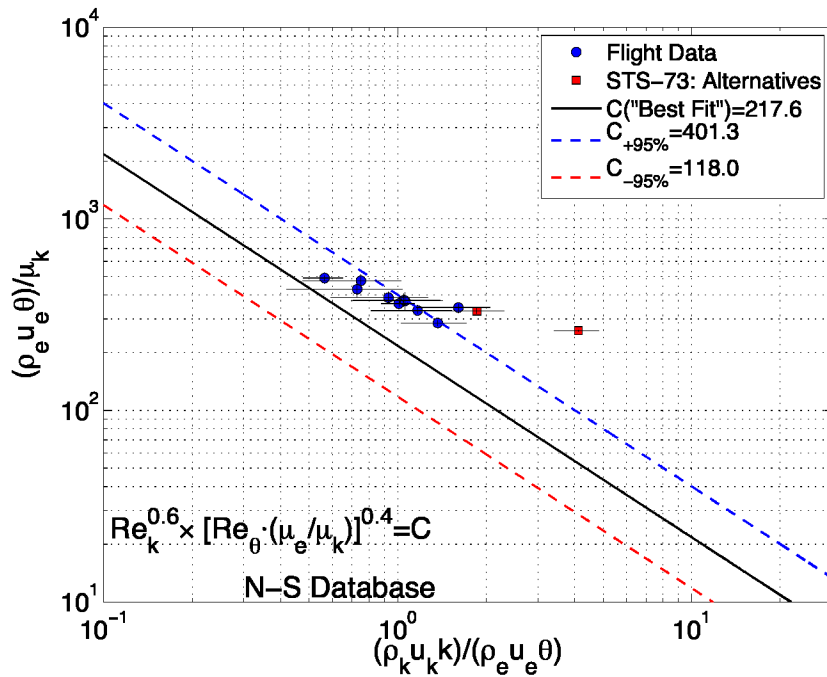


Figure 20. Flight data plotted in correlation space (PC#7) along with correlation curves derived from ensemble of facility dependent and flight data (N-S database).

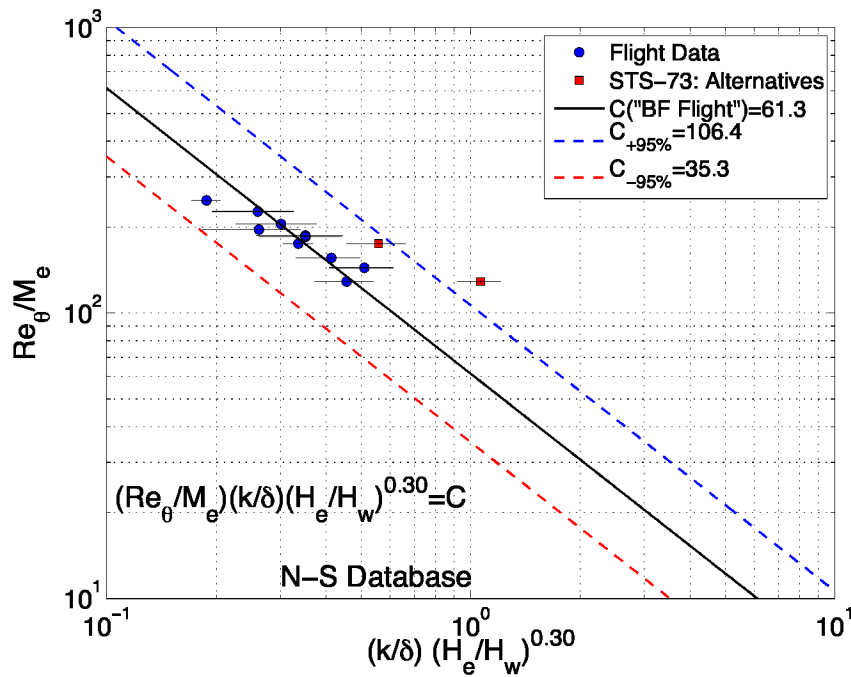


Figure 21. Plot showing flight data (assumes 95% confidence levels for quoted  $k$  values) and correlation curves with constants recommended by the Aeroheating Panel for PC#5.

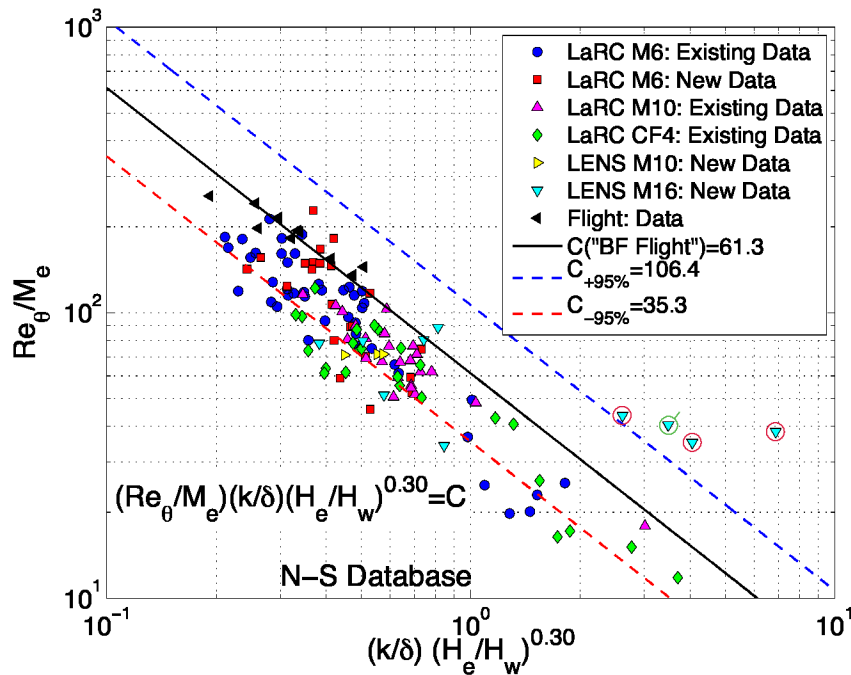


Figure 22. Plot showing ground-based data, flight data, and correlation curves (using constants recommended by the Aeroheating Panel) for PC#5.

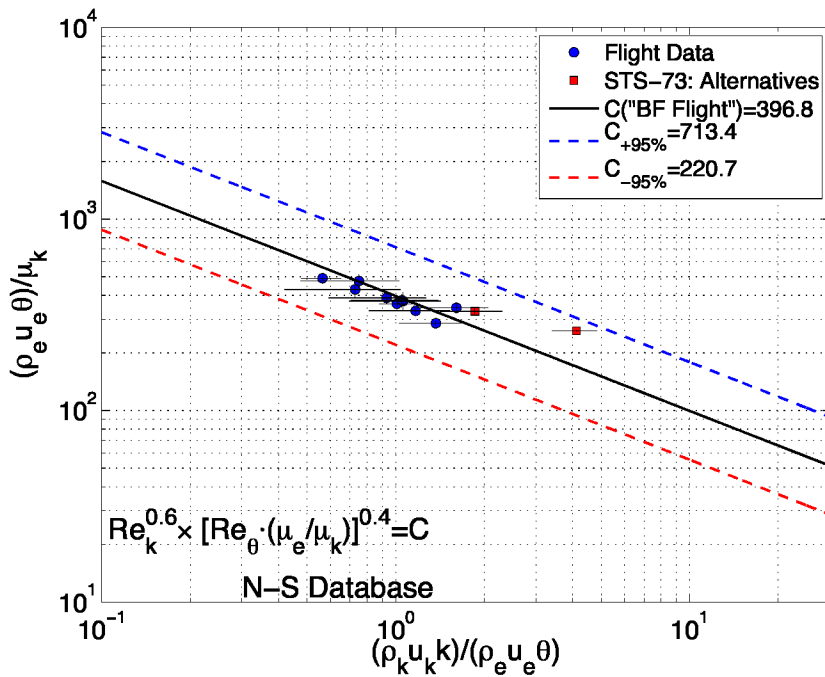


Figure 23. Plot showing flight data (assumes 95% confidence levels for quoted  $k$  values) and correlation curves with constants recommended by the Aeroheating Panel for PC#7.

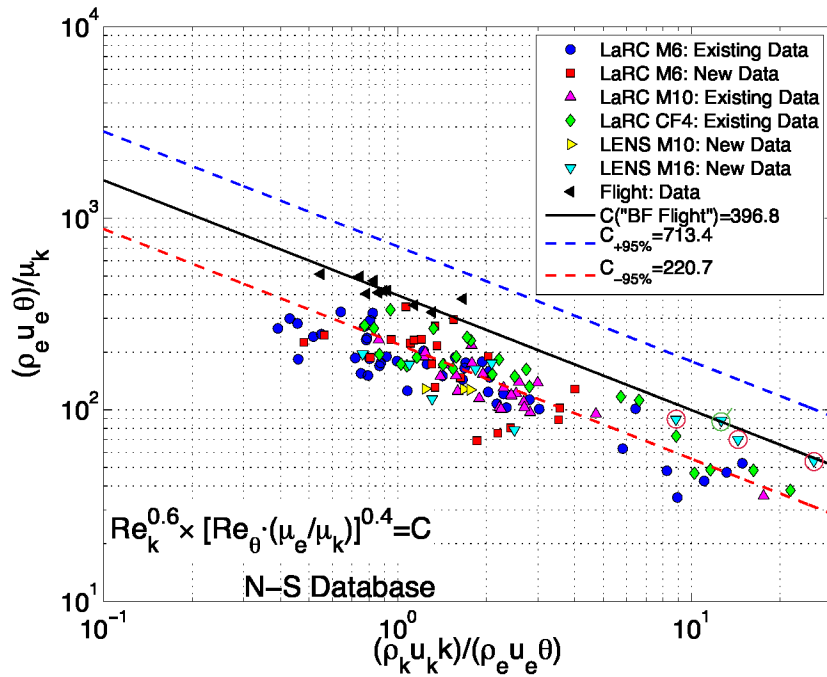


Figure 24. Plot showing ground-based data, flight data, and correlation curves (using constants recommended by the Aeroheating Panel) for PC#7.

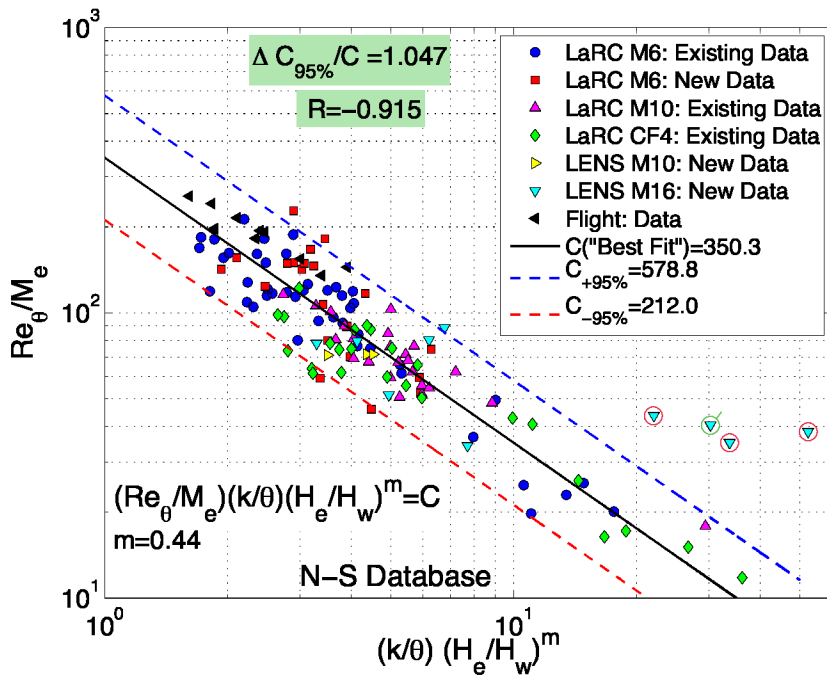


Figure 25. Ensemble of facility dependent data and flight data based on N-S database for correlation  $Re_{\theta}/M_e \times (k/\theta)(H_e/H_w)^{0.44} = C$ .

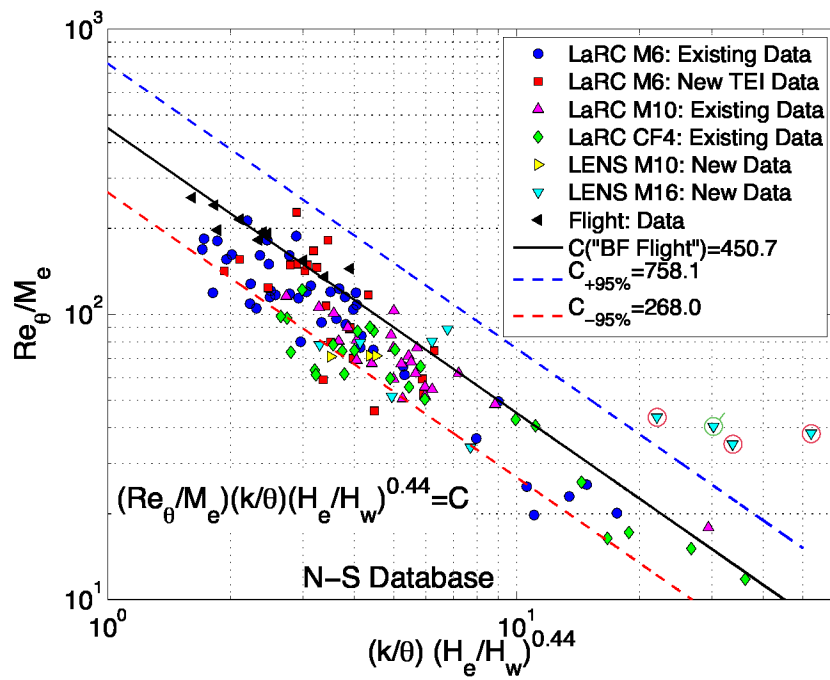


Figure 26. Plot showing ground-based data, flight data, and correlation curves for correlation  $Re_{\theta}/M_e \times (k/\theta)(H_e/H_w)^{0.44} = C$  based on coefficients derived from the methodology of the Aeroheating Panel.

| REPORT DOCUMENTATION PAGE   |                             |  | Form Approved<br>OMB No. 0704-0188                                   |   |
|---|-----------------------------|--|--|---|
| <p>The public reporting burden for this collection of information is estimated to average 1 hour per response, including the time for reviewing instructions, searching existing data sources, gathering and maintaining the data needed, and completing and reviewing the collection of information. Send comments regarding this burden estimate or any other aspect of this collection of information, including suggestions for reducing this burden, to Department of Defense, Washington Headquarters Services, Directorate for Information Operations and Reports (0704-0188), 1215 Jefferson Davis Highway, Suite 1204, Arlington, VA 22202-4302. Respondents should be aware that notwithstanding any other provision of law, no person shall be subject to any penalty for failing to comply with a collection of information if it does not display a currently valid OMB control number.</p> <p><b>PLEASE DO NOT RETURN YOUR FORM TO THE ABOVE ADDRESS.</b></p>   |                             |  |  |   |
| <b>1. REPORT DATE (DD-MM-YYYY)</b><br>01-12-2009  |                             | <b>2. REPORT TYPE</b><br>Technical Publication |  | <b>3. DATES COVERED (From - To)</b><br>10/2000-9/2002 |
| <b>4. TITLE AND SUBTITLE</b><br>Version 2 of the Protuberance Correlations for the Shuttle-Orbiter Boundary Layer Transition Tool   |                             |  | <b>5a. CONTRACT NUMBER</b>   |   |
|   |                             |  | <b>5b. GRANT NUMBER</b>  |   |
|   |                             |  | <b>5c. PROGRAM ELEMENT NUMBER</b>                                    |   |
| <b>6. AUTHOR(S)</b><br>Rudolph A. King, Michael A. Kegerise and Scott A. Berry  |                             |  | <b>5d. PROJECT NUMBER</b>  |   |
|   |                             |  | <b>5e. TASK NUMBER</b>   |   |
|   |                             |  | <b>5f. WORK UNIT NUMBER</b><br>599489.02.07.07.04.11.01              |   |
| <b>7. PERFORMING ORGANIZATION NAME(S) AND ADDRESS(ES)</b><br>NASA Langley Research Center<br>Hampton, Virginia 23681-2199   |                             |  | <b>8. PERFORMING ORGANIZATION REPORT NUMBER</b><br>L-19791           |   |
| <b>9. SPONSORING/MONITORING AGENCY NAME(S) AND ADDRESS(ES)</b><br>National Aeronautics and Space Administration<br>Washington, DC 20546-0001  |                             |  | <b>10. SPONSOR/MONITOR'S ACRONYM(S)</b><br>NASA                      |   |
|   |                             |  | <b>11. SPONSOR/MONITOR'S REPORT NUMBER(S)</b><br>NASA/TP-2009-215951 |   |
| <b>12. DISTRIBUTION/AVAILABILITY STATEMENT</b><br>Unclassified-Unlimited<br>Subject Category 16<br>Availability: NASA CASI (443) 757-5802   |                             |  |  |   |
| <b>13. SUPPLEMENTARY NOTES</b><br>An electronic version can be found at <a href="http://ntrs.nasa.gov">http://ntrs.nasa.gov</a> .   |                             |  |  |   |
| <b>14. ABSTRACT</b><br>Orbiter-specific transition data, acquired in four ground-based facilities (LaRC 20-Inch Mach 6 Air Tunnel, LaRC 31-Inch Mach 10 Air Tunnel, LaRC 20-Inch Mach 6 CF <sub>4</sub> Tunnel, and CUBRC LENS-I Shock Tunnel) with three wind tunnel model scales (0.75, 0.90, and 1.8%) and from Orbiter historical flight data, have been analyzed to improve a pre-existing engineering tool for reentry transition prediction on the windward side of the Orbiter. Boundary layer transition (BLT) engineering correlations for transition induced by isolated protuberances are presented using a laminar Navier-Stokes (N-S) database to provide the relevant boundary-layer properties. It is demonstrated that the earlier version of the BLT correlation that had been developed using parameters derived from an engineering boundary-layer code has improved data collapse when developed with the N-S database. Of the new correlations examined, the proposed correlation 5, based on boundary-layer edge and wall properties, was found to provide the best overall correlation metrics when the entire database is employed. The second independent correlation (proposed correlation 7) selected is based on properties within the boundary layer at the protuberance height. The Aeroheating Panel selected a process to derive the recommended coefficients for Version 2 of the BLT Tool. The assumptions and limitations of the recommended protuberance BLT Tool V.2 are presented. |                             |  |  |   |
| <b>15. SUBJECT TERMS</b><br>Shuttle Orbiter, hypersonic boundary layer transition, roughness-induced transition   |                             |  |  |   |
| <b>16. SECURITY CLASSIFICATION OF:</b>  |                             |  | <b>17. LIMITATION OF ABSTRACT</b><br><br>UU                          | <b>18. NUMBER OF PAGES</b><br><br>58                  |
| <b>a. REPORT</b><br><br>U   | <b>b. ABSTRACT</b><br><br>U | <b>c. THIS PAGE</b><br><br>U                   |  |   |
|   |                             |  | <b>19b. TELEPHONE NUMBER (Include area code)</b><br>(443) 757-5802   |   |



